Evaluating the Potential of Distribution of Relaxation Times Analysis for Plant Agriculture

Maxime Van Haeverbeke*[,1], Bernard De Baets and Michiel Stock

KERMIT, Department of Data Analysis and Mathematical Modelling, Ghent University, Coupure links 653, Ghent, 9000, Belgium

ARTICLE INFO

Keywords:

Electrochemical Impedance Spectroscopy

Distribution of Relaxation Times

Plant physiology

Agriculture

ABSTRACT

The analysis of a Distribution of Relaxation Times (DRT) has proven to be extremely effective for the study of electrochemical power sources. Biological systems are non-inductive, making them very suitable candidates for DRT analysis, as demonstrated by recent research. In this work, we conduct the first evaluation of DRT analysis in agricultural applications. We revisit published equivalent electrical circuit parameter data to evaluate the potential of DRT analysis for various plant electrochemical impedance spectroscopy applications. We investigate the advantages and limitations of adopting this emerging analysis method as an impedance modelling strategy for the electrochemical characterisation of plants. We illustrate its promise by comparing it with the standard methods using simulations and measurements published in the literature on fruit ripening, plant stress, and post-harvest processing of agricultural products. This study highlights the potential of DRT analysis as an effective modelling strategy for impedimetric system characterization in agriculture, with promising advantages over standard techniques.

1. Introduction

Electrochemical impedance spectroscopy (EIS) is an effective, rapid, non-destructive, inexpensive, *in situ*, and real-time plant characterisation method. In its commonly applied potentiostatic form, EIS consists of a small alternating voltage input $V(f)$, where f is the frequency applied to a (bio-)electrochemical system under test. The input $V(f)$ gives rise to an alternating current $I(f)$ flowing through the system. The electrical elements in the system impede the current with a total impedance of $Z(f)$ according to the generalised Ohm law to alternating current:

$$Z(f) = \frac{V(f)}{I(f)} = |Z(f)|(\cos(\phi(f)) + j\sin(\phi(f))), \tag{1}$$

where $|Z(f)|$ is the magnitude of the impedance, $\phi(f)$ is the phase angle between the current and the voltage, and j is the imaginary unit. The value of the impedance depends on the system's electrochemical properties and on the applied frequency f. Measuring $Z(f)$ over a range of frequencies gives rise to an electrochemical impedance spectrum containing substantial information on various properties of the system under test. EIS has been used in many agricultural applications, including the monitoring of various forms of abiotic and biotic stress [1, 2], nutritional status [3, 4], and physiological processes [5, 6]. Equivalent Electrical Circuits (EEC) are currently the standard tools used for the analysis and interpretation of EIS measurements.

The analysis of electrochemical systems with the Distribution of Relaxation Times (DRT) has made great strides in the last five years. As expected, this happened in the most prominent EIS application domain: electrochemical power sources, in particular fuel cells and Li-ion batteries. Numerous studies have been published in these areas [7, 8]. There are, however, several challenges associated with this method. These include the requirement of high-quality data with limited noise and the sensitivity to the appropriate choice of hyper-parameters. We discuss these in detail in Section 2.

To date, the application of DRT analysis to biological EIS measurements remains limited. Ramirez–Chavarria *et al.* [9, 10] initially tested the method for analyzing rat organ tissues. Afterwards, the same authors used the method for

*Corresponding author. M. Van Haeverbeke: Department of Data Analysis and Mathematical Modelling, Ghent University, Coupure links 653, Ghent, 9000, Belgium.

maxime.vanhaeverbeke@ugent.be (M. Van Haeverbeke)

ORCID(s): 0000-0001-7938-1675 (M. Van Haeverbeke); 0000-0002-3876-620X (B. De Baets); 0000-0003-0903-6061 (M. Stock)

Mathematical Notation

β	Regression coefficient
$\gamma(\log \tau)$	Relaxation time distribution function (logarithmically spaced frequencies)
λ	Regularization hyperparameter
$\boldsymbol{\Theta}$	Vector of weights θ
$\mathbf{A}^{\mathrm{Im}}$	Matrix for DRT calculation using the imaginary part of EIS measurements
$\mathbf{A}^{\mathrm{Re}}$	Matrix for DRT calculation using the real part of EIS measurements
$\phi(f)$	Phase angle
ϕ_μ	Radial basis function with shape factor μ
τ	Relaxation time
θ	Weight in Tikhonov regularization
C	Capacitance
$C_{\%}$	Nutrient concentration
f	Frequency
F_{I}	Internal penetration force
$g(\tau)$	Relaxation time distribution function
$I(f)$	Current
j	Imaginary unit
$J(\cdot)$	Objective function
P	Porosity
R	Resistance
R^2	Coefficient of determination
R_{days}	Days of fruit ripening
$V(f)$	Voltage
$Z(f)$	Impedance
$Z^{\mathrm{Im}}(f)$	Imaginary part of impedance
$Z^{\mathrm{Re}}(f)$	Real part of impedance
Z_{EXP}	Experimental impedance measurements
Z_{DRT}	Reconstructed impedance

sensing the concentration of biological cells in suspension [11], showing that DRT analysis can thoroughly characterise biological cell suspensions in highly conductive culture media. The authors state that a simple parametric model can be derived from the DRT to decode the biological cell suspension's electrochemical properties. The DRT of a biological cell suspension has three distinct peaks, the first of which has a time constant that predicts the cell's concentration well. Next, Shi *et al.* [12] applied DRT analysis to characterise the relaxation mechanisms of rat liver epithelial cells in a monolayer. The above discussion shows that recent biological DRT applications hold promise, although they are currently still very limited in number. To the best of our knowledge, so far there have been no studies evaluating the

use of DRT analysis for plant applications. A straightforward transfer of DRT analysis from electrical power sources to a biological application is the novel application of DRT analysis to microbial fuel cells [13].

The remainder of this paper is organised as follows. Section 2 introduces the DRT analysis method, with an elucidation of the estimation of the DRT using Tikhonov regularisation and a discretisation with radial basis functions. Section 3 provides a brief literature review of the EIS applications in plant agriculture that are relevant to this work. The data collection and simulation approach used for this work is described in Secion 4. In Section 5, we conduct a simulation-based evaluation in various plant applications making use of published data in the plant EIS literature. The freely available accompanying software that was developed for the purpose of this paper is briefly described in Section 6. The findings are discussed and placed into context in Section 7, followed by a conclusion in Section 8, along with some perspectives for future research.

2. The Distribution of Relaxation Times analysis method

The electrical components of an electrochemical system become polarised under the influence of an external electric field. This polarisation depends on the system's nature and the electric field's frequency. Upon removal of the electric field, depolarisation (dielectric relaxation) occurs. This depolarisation is characterised by a specific relaxation time constant τ. Almost all electrochemical processes are polarisation processes with associated relaxation times [14]. The Distribution of Relaxation Times (DRT) [15], sometimes also referred to as the Distribution Function of Relaxation Times (DFRT), is an emerging distributed parametric tool that sheds light on hard-to-interpret cases where the system-under-test involves electrochemical processes with similar time constants [16]. In this section, we first consider the definition of the DRT in Section 2.1 and then discuss the Tikhonov-regularisation-based DRT deconvolution used in this work in Section 2.2.

2.1. Distribution of Relaxation Times definition

The DRT analysis method is often reported as being model-free, though strictly speaking, it assumes a very general model consisting of an Ohmic resistance connected to an infinite number of serially connected Voigt circuits (i.e., parallelly connected resistor and capacitor elements) [17]. This model is displayed in Figure 1A. From Kirchhoff's laws and the expressions for the impedance over resistors and capacitors, the impedance of a single resistance parallelly connected to a capacitance is given by

$$Z_{\mathrm{RC}} = \frac{R}{1 + 2\pi j f RC}\,, \tag{2}$$

where R is the resistance, C the capacitance, and f the interrogated input frequency. Thus the impedance of a resistor in series with N such Voigt elements is given by

$$Z_{\mathrm{Voigt_n}} = R_0 + \sum_{n=1}^{N} \frac{R_n}{1 + 2\pi j f \tau_n}\,. \tag{3}$$

DRT analysis assumes an infinite number of Voigt circuits, each characterised by its own relaxation time τ, and associates them with their distribution function $g(\tau) \geq 0$. Following this reasoning, we arrive at the equation relating the distribution of relaxation times to the impedance of a given system:

$$Z_{\mathrm{DRT}}(f) = R_\infty + \int_0^\infty \frac{g(\tau)}{1 + 2\pi j f \tau}\mathrm{d}\tau\,. \tag{4}$$

Here, R_0 and R_n from Eq. (3) are absorbed into R_∞, the high-frequency intercept of the impedance spectrum (i.e., the value of the real-valued impedance at the point where the spectrum crosses the horizontal axis in the Nyquist plot), and $g(\tau)$, respectively. Frequency-domain impedance measurements are deconvoluted to the time constant domain, where various relaxation processes and their time constants can be examined. In addition, DRT analysis can also aid in various aspects of equivalent circuit analysis such as EEC topology establishment or confirmation [18, 19], providing reasonable initial values for the parameter optimization methods that require them [20], and EEC parameterisation [21].

2.2. Estimating the DRT using Tikhonov Regularisation

Solving Eq. (4) for $g(\tau)$ is an ill-posed problem (i.e., it is a Fredholm integral equation of the first kind), meaning there might not be a unique distribution function for a given impedance spectrum. As a result, one requires sophisticated estimation strategies to solve the inverse problem adequately. To this end, we approximate Eq. (4) with a well-posed variant. This approximation is currently an active area of research with a variety of proposed strategies, including Monte Carlo methods [22], evolutionary programming [23], Fourier filtering [24], Tikhonov regularisation (cfr., ridge regression) [25], hierarchical Bayesian regularisation [26], and supervised deep learning [27]. One of the most popular approaches that has proven to work well is a basis function discretisation followed by ridge regression [28]. In this work, we adopt this approach for the DRT calculation, and implement it in the Julia programming language [29] (see Section 6).

When the impedance measurements are collected at logarithmically-spaced frequencies, a change of variables ($\tau \mapsto \log \tau$) is in order (where log refers to the natural logarithm):

$$Z_{\mathrm{DRT}}(f) = R_\infty + \int_{-\infty}^{\infty} \frac{\gamma(\log \tau)}{1 + 2\pi j f \tau} \mathrm{d} \log \tau \,, \tag{5}$$

where $\gamma(\log \tau) = \tau g(\tau)$. $Z_{\mathrm{DRT}}(f)$ is often referred to as the *reconstructed impedance*, as the goal is to find an appropriate function $\gamma(\log \tau)$ such that a given set of experimental impedance measurements Z_{EXP} is reconstructed by the right-hand side of Eq. (5). Some authors conduct a normalization, imposing the constraint $\int_{-\infty}^{\infty} \gamma(\log \tau) \mathrm{d} \log \tau = 1$ [17]. This way, the resulting distribution function is a valid probability density function. We opted not to include this constraint because we found that the amplitude of the DRT provides useful information about both the relative importance of different relaxation processes and the absolute magnitude of the impedance allotted to those processes across different measurements. In this case, the DRT's amplitude may be a useful feature when modelling the properties of an electrochemical system (see Section 4.2). A discretisation of the distribution function $\gamma(\log \tau)$ is required before we can estimate the DRT. We use the radial basis function discretisation proposed by Wan *et al.* [28]:

$$\gamma(\log \tau) = \sum_{n=1}^{N} \theta_n \phi_\mu(|\log \tau - \log \tau_n|) \,, \tag{6}$$

where $\phi_\mu(|\log \tau - \log \tau_n|)$ is a radial basis function with shape factor μ. Previous work has demonstrated that the Gaussian radial basis function $\phi_\mu(x) = \exp(-(\mu x)^2)$ works well for DRT [11, 12], which is why we chose to adopt it. Equation (5) describes the distribution of relaxation times $\gamma(\log \tau)$ as a sum of N radial basis functions centered at relaxation times τ_n and weighed by $\theta_n \geq 0$. Physically, one can interpret this representation as N generalised RC circuits with a relaxation time τ_n surrounded by a distribution of infinitesimal Voigt circuits. Figures 1B, C, and D display exemplary plots of what the Gaussian radial basis functions, the values of θ_n, and the resulting DRT may look like in practice.

Combining Eqs. (5) and (6), we get the expression for impedance ($Z_{\mathrm{DRT}}(f)$) reconstructed using the distribution function discretised by radial basis functions :

$$\begin{aligned} &R_\infty + \int_{-\infty}^{\infty} \sum_{n=1}^{N} \theta_n \frac{\phi_\mu(|\log \tau - \log \tau_n|)}{1 + 2\pi j f \tau} \mathrm{d} \log \tau \\ &= R_\infty + \sum_{n=1}^{N} \theta_n \int_{-\infty}^{\infty} \frac{\phi_\mu(|\log \tau - \log \tau_n|)}{1 + 2\pi j f \tau} \mathrm{d} \log \tau \,. \end{aligned} \tag{7}$$

The reconstructed impedance $Z_{\mathrm{DRT}}(f)$ can be written as

$$Z_{\mathrm{DRT}}(f) = Z_{\mathrm{DRT}}^{\mathrm{Re}}(f) + j Z_{\mathrm{DRT}}^{\mathrm{Im}}(f) \,, \tag{8}$$

with real part $Z_{\mathrm{DRT}}^{\mathrm{Re}}(f)$ and imaginary part $Z_{\mathrm{DRT}}^{\mathrm{Im}}(f)$.

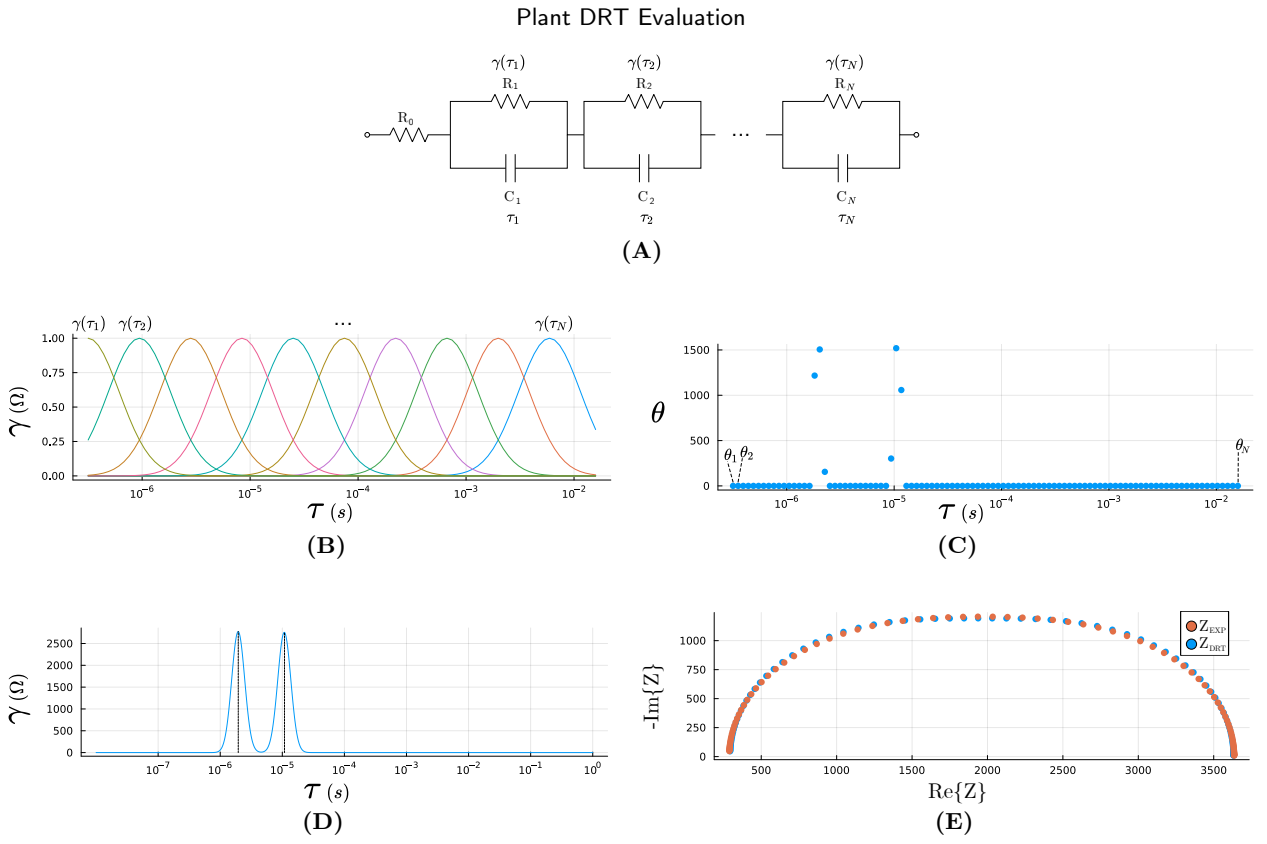

Figure 1: An overview of the DRT inversion from the frequency domain to the time-constant domain with discretisation using Gaussian radial basis functions. (A) A series connection of Voigt circuits forms the underlying model of the DRT. Each of the n Voigt subcircuits entails its corresponding contribution to the DRT at τ_n. (B) The DRT is discretised by Gaussian radial basis functions ϕ_μ, generalising the Voigt circuit contributions and allowing the DRT to be defined at $-\inf$ and $\inf$. (C) The weights $\boldsymbol{\Theta}$ resulting from the Tikhonov regularisation given in Eq. (14). The combination of the radial basis functions with the weights $\boldsymbol{\Theta}$ results in the DRT $\gamma(\log\tau)$ of the system displayed in (D). (E) The Nyquist representations of the measurements Z_{EXP} and reconstructed impedance Z_{DRT} after optimization. A fundamental advantage of the DRT can be seen here, as the two relaxation processes cannot be resolved from the Nyquist plots, whereas they are visible in the DRT. The measurements used in this figure are cabbage leaf EIS measurements with a water content of 84%, also displayed in Figure 3.

Multiplication of the numerator and denominator of the integrand in Eq. (7) by $(1 - j\pi 2)$ allows to separate the real and imaginary parts of Z_{DRT}, with $Z^{\text{Re}}_{\text{DRT}}(f)$ given by

$$R_\infty + \sum_{n=1}^{N} \theta_n \int_{-\infty}^{\infty} \frac{\phi_\mu(|\log\tau - \log\tau_n|)}{1 + (2\pi f\tau)^2} \mathrm{d}\log\tau\,, \tag{9}$$

and $jZ^{\text{Im}}_{\text{DRT}}(f)$ by

$$-j\sum_{n=1}^{N} \theta_n \int_{-\infty}^{\infty} \frac{2\pi f\,\phi_\mu(|\log\tau - \log\tau_n|)}{1 + (2\pi f\tau)^2} \mathrm{d}\log\tau\,. \tag{10}$$

When solved numerically, Eq. (8) is written in condensed vector form:

$$\mathbf{Z}_{\text{DRT}} = \mathbf{Z}^{\text{Re}}_{\text{DRT}} + j\mathbf{Z}^{\text{im}}_{\text{DRT}}\,. \tag{11}$$

In Eq. (11), $\mathbf{Z}_{\text{DRT}}$ is the vector of *reconstructed impedance* values for all considered frequencies, with $\mathbf{Z}^{\text{Re}}_{\text{DRT}}$ and $\mathbf{Z}^{\text{im}}_{\text{DRT}}$ its real and imaginary parts. For a frequency vector $\mathbf{F} \in \mathbb{R}^{L\times 1}$ with values $f_1, f_2, \dots, f_L$, the vectors $\mathbf{Z}^{\text{Re}}_{\text{DRT}} \in \mathbb{R}^L$ and $\mathbf{Z}^{\text{im}}_{\text{DRT}} \in \mathbb{R}^L$ are calculated as

$$\mathbf{Z}^{\text{Re}}_{\text{DRT}} = R_\infty \mathbf{1} + \mathbf{A}^{\text{Re}}\boldsymbol{\Theta} \tag{12}$$

$$\mathbf{Z}^{\text{im}}_{\text{DRT}} = j\mathbf{A}^{\text{Im}}\boldsymbol{\Theta}\,, \tag{13}$$

where the values of the vector $\boldsymbol{\Theta} \in \mathbb{R}^N$ are $\theta_1, \theta_2 \dots, \theta_N$, $\mathbf{1}$ is a vector of ones, and the matrices $\mathbf{A}^{\text{Re}} \in \mathbb{R}^{L\times N}$ and $\mathbf{A}^{\text{Im}} \in \mathbb{R}^{L\times N}$ are given by

$$\mathbf{A}^{\text{Re}}_{m,n} = \int_{-\infty}^{\infty} \frac{1}{1+(2\pi)^2 e^{2(x+\log f_n - \log f_m)}} \phi_\mu(|x|)\mathrm{d}x\,,$$

$$\mathbf{A}^{\text{Im}}_{m,n} = \int_{-\infty}^{\infty} \frac{2\pi e^{x+\log f_n - \log f_m}}{1+(2\pi)^2 e^{2(x+\log f_n - \log f_m)}} \phi_\mu(|x|)\mathrm{d}x\,.$$

The above equations were obtained through a change of variables of the integrals in Eq. (9) and (10), respectively. They can be conveniently solved using numerical integration algorithms, such as adaptive Gauss-Kronrod quadrature [30].

In order to approximate the distribution of relaxation times $\gamma(\log\tau)$ using Tikhonov regularisation, we need to find the optimal vector $\boldsymbol{\Theta}$ such that the reconstructed impedance vector $\mathbf{Z}_{\text{DRT}}$ matches the experimentally measured impedance vector $\mathbf{Z}_{\text{EXP}}$ from the (bio)electrochemical system-under-test. This amounts to the minimization of a regularised objective function:

$$J(\boldsymbol{\Theta}) = \|R_\infty \mathbf{1} + \mathbf{A}^{\text{Re}}\boldsymbol{\Theta} - \mathbf{Z}^{\text{Re}}_{\text{EXP}}\|^2 + \|\mathbf{A}^{\text{Im}}\boldsymbol{\Theta} - \mathbf{Z}^{\text{Im}}_{\text{EXP}}\|^2 + \lambda\|\boldsymbol{\Theta}\|^2\,. \tag{14}$$

The last term in Eq. (14) is the regularisation term, where λ is the regularisation hyper-parameter applied in Tikhonov regularisation. In this work, the L_2-norm of the vector $\boldsymbol{\Theta}$ is used to apply regularisation, following the guidelines of Hahn *et al.* [31]. Other possibilities to regularise the objective function are terms proportional to the first or second derivative of $\gamma(\log\tau)$ [12, 28]. The minimization of Eq. (14) is adequately achieved using the Broyden–Fletcher–Goldfarb–Shanno algorithm [32]. In a Kramers–Kronig compliant system, adhering to the linearity, causal, and time-invariance quality criteria for EIS measurements [33], the DRT can also be calculated using only the real or only the imaginary parts of the measurements. This means that the first or second terms in Eq. (14) can be dropped. In some cases, it can be advisable to use only the real or imaginary parts of the measurements (e.g., due to some measurement quality considerations). Usually, using the complete Eq. (14) is advisable [31]. The choice of the regularisation hyper-parameter λ has been the subject of extensive study. Large values of λ cause extensive smoothing of the DRT, resulting in flatter and wider peaks. If the value of λ is too large, it can cause peaks to disappear, resulting in a misinterpretation of the system under investigation. Conversely, excessively small values of λ should also be avoided, as these give rise to artifacts and spurious peaks in the DRT. Some developed automatic tuning procedures include the minimization of the discrepancy between $\boldsymbol{\Theta}$ calculated using real and imaginary parts of measurements [34], real and imaginary Z_{DRT} cross-validation [34], the L-curve (offset) method [35, 36], and generalised cross-validation methods [37]. Despite these efforts, it remains advisable to be cautious when using these automated procedures, as they have been reported to provide inconsistent results [19, 31]. The shape factor μ in the DRT discretised by radial basis functions serves as another regularisation parameter to be selected. This shape factor is related to the full width at half maximum of the radial basis functions. Decreasing μ causes flattening of the DRT, which is the opposite effect of decreasing λ.

3. Impedance spectroscopy in plant agriculture

While the potential of EIS for characterising the physiological processes of plants was already evident in the middle of the previous century, recent decades have seen a substantial increase in studies exploiting the vast information contained in impedance spectra for plant agricultural applications [38]. Many such applications have been investigated, ranging from fruit ripeness to the effect of post-harvest processing operations on the quality and nutritional value of plant products. This section briefly reviews the literature on the various applications considered in this work. The considered applications are the impedimetric evaluation of fruit ripening, abiotic stress, seed germination and quality, plant nutrition, and post-harvest processing operations. A number of the described applications are considered in Section 5, where we evaluate DRT analysis in plant agriculture.

3.1. Fruit ripening

Chowdhury *et al.* [6] conducted EIS measurements on *Citrus reticulata* (mandarin oranges) to assess the feasibility of inferring the ripeness of fruits based on their impedance spectra. To this end, the authors non-invasively measured the impedance spectra on six consecutive days. The authors observed an increasing impedance magnitude and variations in the phase angle during the ripening period. An EEC-based analysis was conducted on each day of the experiment.

Harker and Forbes. [39] investigated the changes in impedance spectra during the ripening of *Diospyros kaki* L. (persimmon) fruit. They conducted measurements after 1, 25, and 35 days. The authors observed an initial increase of the impedance between 1 and 21 days, followed by a substantial decrease after 35 days. Using an EEC, an increase in the cell wall, cytoplasm, and vacuole resistance was reported during the first 21 days. After 31 days, a substantially lowered cell wall resistance and an increased membrane capacitance were reported. The initial increase before 21 days of ripening was reported to reflect decreases in the concentration of mobile charged species or an increase in insulatory compounds such as sugars. The disintegration of the plant cell's compartmentalization at late-stage ripening grants low-frequency current access to the cells, which is reflected in a substantially decreased impedance.

The same authors investigated the changes in impedance spectra during the ripening of *Prunus persica* L. (nectarines) [40]. Here, they measured the respective impedance spectra of unripe and ripe nectarines and reported a decrease in all resistances and capacitances based on the change in EEC model parameters.

3.2. Abiotic stress

Zhang and Willison impedimetrically evaluated the effect of freeze-thaw injury on the electrical properties of *Daucus carota* L. (carrot) root tissues [41]. The authors reported that the discharge of electrolytes from cells led to a reduction in extracellular impedance. The freeze-thaw cycles to -3 or -6°C caused the extracellular resistance and vacuole interior resistance of the carrot tissues to halve relative to the control values, while the cytoplasmic resistance further decreased to a third of the control value. Tonoplast and plasma membrane capacitances were not strongly influenced by these non-injurious freeze stresses. At lower temperatures, a large decrease in all resistances and capacitances was observed due to rupturing of protoplasts.

Watanabe *et al.* [42] evaluated the effect of mechanical stress on the resulting impedance spectra through drop shock bruising of *Pyrus pyrifolia* (Japanese pear), followed by conducting EIS measurements. The authors defined a damage score to quantify damage to the fruits after drop shock treatment, where a score of 1 corresponds to the control samples without injury, and a score of 5 corresponds to an injury covering half of the fruit's bottom surface. Physical damage is an important factor influencing the quality of fruits when they are being processed, handled, and distributed. The authors reported a reduced cell membrane capacitance due to damaged membranes after injury and a reduced extracellular resistance due to leakage of the conducting electrolytes from the protoplast into the apoplast of the fruit tissue, as well as a slight increase of the intracellular resistance.

3.3. Seed germination

A generally applicable, fast, non-destructive and cheap method for evaluating seed quality is important for efficient agricultural production and determining optimal storage conditions to delay the decline in seed vigour and viability. The standard germination test typically takes over a week [43], and the destructive assays based on 2,3,5-triphenyl tetrazolium chloride (TTC) take 1-2 days [44]. X-ray measurements are fast and reliable for assessing seed viability [45], but they are expensive and are only effective for certain seed types. Furthermore, X-ray measurements involve exposure to radiation, which may be a concern for seed samples that need to be used for further breeding or research.

Ackmann and Seitz [46] were the first to analyse seed germination with EIS in 1984. The authors reported decreasing characteristic frequencies during seed germination in their study of *Ricinus communis* L. (castor bean). Paine *et al.* [47] and Repo *et al.* [48] corroborated these results and linked them to changed moisture content during seed germination, while evaluating EIS as a method to assess seed quality. Here, the germinability of *Phaseolus vulgaris* L. (snap bean) seeds was impedimetrically evaluated on fresh seeds and artificially aged seeds with reduced germination potential. A moisture content of 45% was deemed optimal for classifying a lot of snap bean seeds into germinable and non-germinable ones.

Vozary *et al.* [49] assessed the electrochemical properties of *Phaseolus vulgaris* L. (snap beans) and *Glycine max* L. (soybeans) in different states of viability and vigour at a fixed seed moisture content of 45%. Through an EEC model analysis, they found that the quality of the seeds has a measurable impact on their (non-invasively measured) impedance spectrum. The physiological state of the seeds, in turn, strongly relates to the seedling's quality.

3.4. Plant nutrition

Nitrogen (N), phosphorus (P), and potassium (K) are essential chemical elements of interest for crop quality and growth. They are the most important macronutrients in modern agricultural fertilisers [50]. The effective and non-invasive measurement of the concentrations of these nutrients holds promise for precision agriculture and advanced fertiliser management. Besides the traditional, destructive chemical plant nutrition assessment methods, methods to interrogate the NPK-nutrition status of plants typically rely on the measurement of optical properties on the leaf or canopy level. A criticism of these methods is that they are sensitive to environmental conditions [4]. EIS is capable of meeting the modern agricultural standards of being rapid, non-destructive, and real-time. The quick and precise identification of a plant's nutrient status prior to visible symptoms is crucial for optimal fertiliser application and maximum productivity. Recently, some studies have started to explore the potential of EIS-based methods to assess the NPK status of plants. Meiqing *et al.* [51] conducted *Solanum lycopersicum* (tomato) leaf measurements for the purpose of detecting the phosphorus nutrition level. In another study, the same authors did similar measurements on tomato plants for the assessment of the nitrogen nutrition level [4]. Jinyang *et al.* [52] experimentally analysed tomato plants' potassium nutrition levels through EIS measurements. Basak *et al.* conducted a similar study to determine the leaf nitrogen content of corn, wheat, canola, and soybeans. They also performed a linear regression with a backward selection of the many impedance features available. High correlations were reported with their linear models containing many features. Evaluation of the models on separate data, external to the calibration dataset, was not done in their work.

3.5. Processing of plant products

Due to their ease of storage and convenience, processed foods, including dried, precooked, and frozen vegetables, are in high demand. Proper safety and quality assurance are essential for such food products, and EIS has great potential for conducting such a real-time, rapid, automatable, cheap, and non-destructive quality assessment. To this end, several research works have proposed EIS-based methods. Heat treatment is a common operation in food processing. Imaizumi *et al.* [53] subjected *Solanum tuberosum* L. (potato) tubers to hot water treatment over a range of temperatures. They found that EIS is capable of describing the textural changes and softening of potatoes during heat treatment. The authors conducted an EEC-based analysis and reported decreases in the cell membrane capacitance as a result of membrane damage (and the resulting loss of turgor pressure) and confirmed this through Confocal Laser Scanning Microscopy (CLSM) with Dil staining and penetration force testing.

Watanabe *et al.* [54] investigated the mechanical and bioelectrochemical properties of *Spinacia oleracea* L. (spinach) after short-duration heat treatment (blanching) using steam at 100°C. Tensile fracture tests and EIS measurements were conducted along with EEC model parameter fitting after heat treatment. The authors reported decreased extracellular resistance and cell membrane capacitance after heat treatment.

4. Materials and methods

Relaxation times of plant impedance spectra have already been established as valuable features to describe plant tissues' physiological and morphological states. However, traditional calculation methods of these features are based on finding the peaks in the Nyquist plots of impedance spectra with a limited frequency resolution or are dependent on proposed (biased) equivalent electrical circuit models. Ozier–Lafontaine and Bajazet [55] report changes in the relaxation time constants of a tomato root system. The authors already anticipated the limitations of a graphical approach to identifying relaxation times and the need for effective numerical deconvolution methods. The novel DRT analysis method does not require equivalent circuit identification and parameterization in the traditional sense and is calculated directly from the impedance measurements. Furthermore, it is more precise, allowing for electrochemical relaxation processes with similar relaxation times to be resolved, which allows it to analyse impedance spectra in greater depth. This section contains a description of the *semi-synthetic* data collection (Section 4.1) and the conducted experiments for the evaluation of the potential of DRT analysis for plant applications (Section 4.2).

4.1. Collecting EIS measurements

We conducted an extensive literature search to gather a variety of plant EIS measurements that satisfy our imposed quality criteria. As raw EIS data of sufficient quality is frequently unavailable, the measurements were indirectly collected through the reported frequency ranges, the equivalent circuit topologies, and the corresponding parameter values. As we wish to simulate the impedance measurements as accurately as possible, more complex (albeit appropriate) circuits with lower fitting errors are preferred, such as models containing ZARC elements, the

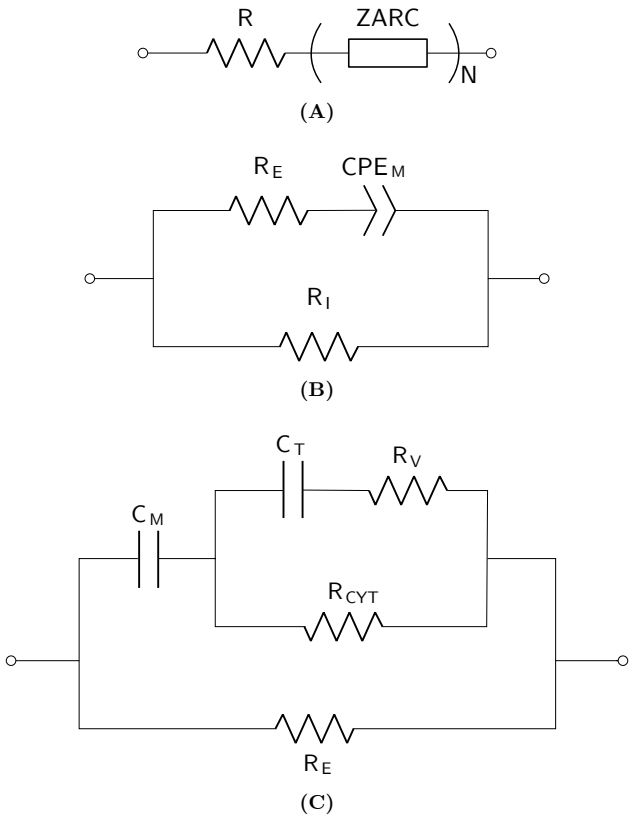

Figure 2: Equivalent Electrical Circuits featuring in the experiments. (A) A resistor serially coupled to N ZARC elements, each modelling a different segment of the considered plant part. (B) The fractionalised single shell model, where R_{E} is the extracellular resistance, R_{I} is the intracellular resistance, and $\mathrm{CPE}_{\mathrm{M}}$ is the constant phase element modelling the capacitance of the cell membrane. (C) The double shell model, where C_{M} denotes the cell membrane capacitance, C_{T} the tonoplast capacitance, R_{E} the extracellular resistance, R_{I} the intracellular resistance, and R_{V} the vacuolar resistance.

double shell model, and the fractional single shell model displayed in Figure 2A, B, and C, respectively. The measured frequency range and equivalent electrical circuit parameters were collected, after which 100 logarithmically spaced impedance measurements were simulated using our previously published `EquivalentCircuits.jl` software [56]. The impedance expressions of these equivalent circuits are derived through the application of Kirchhoff's laws and the impedance expressions of the circuit components [57]. The obtained measurements were included in this work, provided that (i) a high-quality circuit parameter fit was reported, indicating that the measurements are approximately the same as those simulated using the reported circuit parameters, and (ii) the circuit parameters were clearly reported in tabular or scatter plot form. In the latter case, the parameter values can be reliably obtained using plot digitizing software. In most cases, the results of different literature sources were compared for the examined physiological properties. It has been shown that measurements simulated using equivalent circuits comprised of resistors, capacitors, Warburg elements, and CPE elements are valid impedance spectra conforming to the Kramers–Kronig relations [58].

For the fractional single shell model (displayed in Figure 2B), equivalent capacitance values of the CPE are typically reported for the membrane capacitance. These apparent capacitance values are based on the widely applied mathematical formula proposed by Hsu and Mansfield [59]. The assumptions upon which this formula relies imply that the single main relaxation time response system of homogeneous plant tissues implied through use of the single shell model remains unchanged upon conversion, justifying the use of the apparent capacitance when simulating the measurements for the purpose of the DRT evaluation in this work.

4.2. Simulated case studies from the plant literature

We searched the literature for plant EIS studies relevant to several agricultural applications. These applications are fruit ripening, abiotic stress, seed viability, nutritional status, and post-harvest processing of agricultural products.

Semi-synthetic measurements were procured from selected studies satisfying the criteria described in Section 4.1. The DRT of these measurements was subsequently estimated using the deconvolution approach described in Section 2.2. The λ and μ hyper-parameters were determined manually and using Re-Im cross-validation (see Section 2.2) for each considered case study. The same hyper-parameters were used within a given case study. One of the aspects to be evaluated is whether DRT analysis can provide useful features for statistical inference and predictive models. To this end, linear regression models using DRT features are evaluated for predicting the considered plant properties of interest, where relevant. The quality of the linear regression fits is evaluated using the coefficient of determination R^2. Next, the predictive performance of the linear regression models is evaluated using R^2, based on Leave-One-Out Cross-Validation (LOOCV).

5. Results

An illustrative comparison of the DRT with the traditional EIS representations is given in Section 5.1. The DRT evaluation case studies in various agricultural applications are presented in Section 5.2.

5.1. Comparative overview of EIS representations

Traditional Nyquist and Bode representations are compared with the DRT in Figure 3. The measurements represented in this figure were selected from Zhang and Willison's work [60]. *Brassica oleracea* L. (cabbage) leaf development was impedimetrically analysed by Zhang and willison [60]. These EIS measurements were simulated (see Section 4.1) to illustrate the different EIS representations. The authors found that leaf development was correlated with the parameters of the double shell EEC model (shown in Figure 2C), which they developed [61]. Leaf development manifested itself electrochemically through increased extracellular, cytoplasmic, and vacuole interior resistances along with decreases in the plasma membrane and tonoplast capacitances. The authors measured the water content by weighing the fresh and dried samples. The different EIS representations are displayed in Figure 3. Concerning the water content for the considered measurements, there is no visual relation to be seen in the Nyquist (A) or Bode magnitude (C) representations. Upon careful inspection of the Bode phase plot (D), the frequency at which the phase reaches a minimum provides some information, indicating that the minimum occurs at higher frequencies with increasing water content. Two relaxation processes that were not visible in the Nyquist plots are identified in the DRT (B). These measurements indicate that the relaxation time τ of the second relaxation process (i.e., the second peak) becomes longer with increasing water content. Since Zhang and Willison's experiments, several more recent studies have been conducted regarding the moisture content of plants.

5.2. Case studies in agriculture

The potential of DRT analysis is evaluated through several case studies relevant to agriculture. The case studies considered are fruit ripening, plant stress, seed germination, plant nutrition, and postharvest processing. The conducted DRT evaluations include informative figures. In the cases where sufficient measurements are available, the potential of DRT-based variables to determine properties relevant to plant agriculture is assessed through regression models. For a given quantity Q describing a particular plant property, the following linear regression models are evaluated:

$$Q(\tau_{\text{peak}}) = \beta_0 + \beta_1 \tau_{\text{peak}}\,, \tag{15}$$

$$Q(\gamma(\tau_{\text{peak}})) = \beta_0 + \beta_1 \gamma(\tau_{\text{peak}})\,, \tag{16}$$

$$Q(\tau_{\text{peak}}, \gamma(\tau_{\text{peak}})) = \beta_0 + \beta_1 \tau_{\text{peak}} + \beta_2\, \gamma(\tau_{\text{peak}})\,, \tag{17}$$

$$Q(\tau_{\text{peak}}, \gamma(\tau_{\text{peak}})) = \beta_0 + \beta_1 \tau_{\text{peak}} + \beta_2\, \log_{10} \gamma(\tau_{\text{peak}})\,. \tag{18}$$

Here, $\beta_0, \beta_1, \beta_2$ are the intercept and fitted regression coefficients, while $\tau_{\text{peak}}, \gamma(\tau_{\text{peak}})$ are the respective $\log_{10}$ relaxation time and amplitude of the peak of interest in the DRT. The coefficient of determination $R^2 = 1 - \frac{\text{RSS}}{\text{TSS}}$ (where RSS stands for the residual sum of squares and TSS stands for the total sum of squares) is calculated for these regression models, and the model with the highest R^2 value, given that the included variables are all significant, is reported. We consider a regressor to be significant if the two-sided t-test yields a p-value lower than the conventional threshold of 5%. Information on the statistical significance of the DRT-based variables, their 95% confidence intervals and standard errors can be found in Table 1.

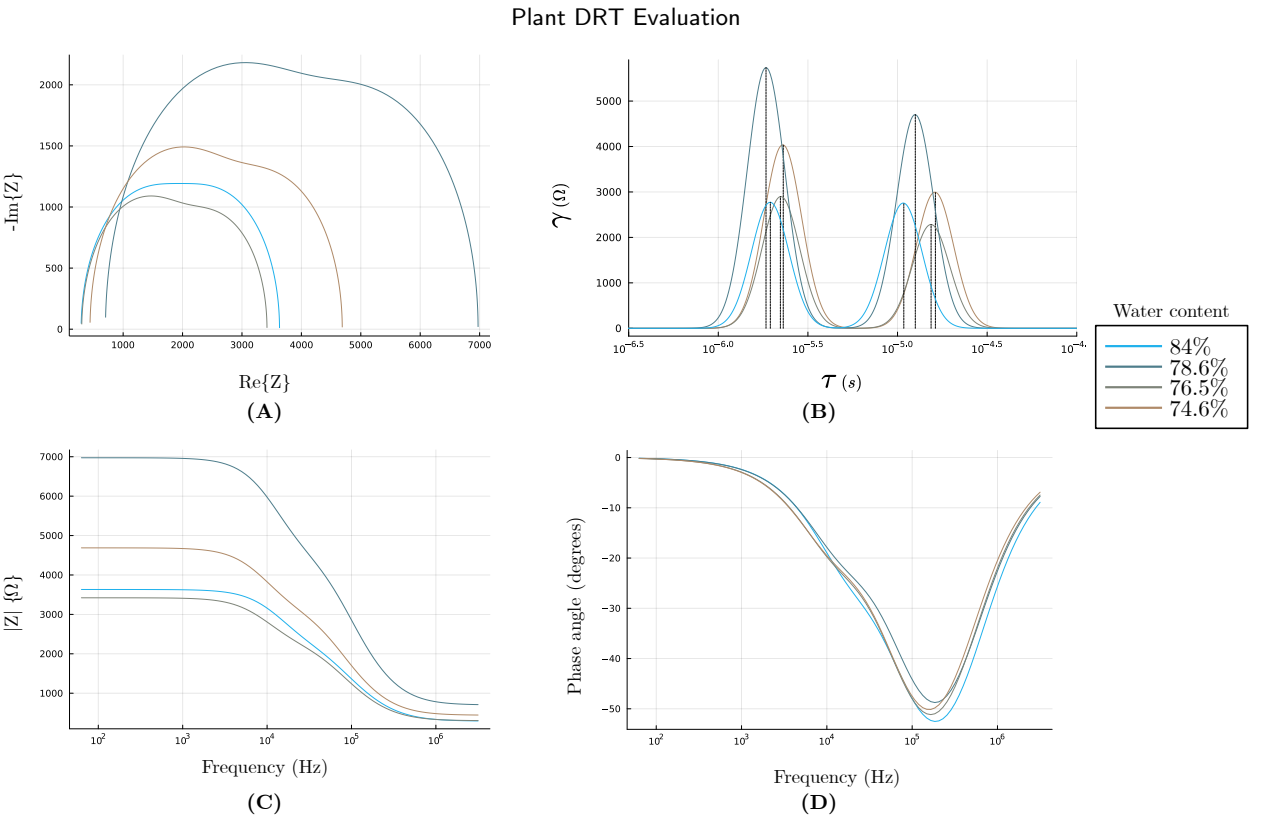

Figure 3: A comparison of the traditional Nyquist and Bode plot EIS representations with the corresponding DRT. (A) Nyquist plots. (B) DRT. (C) Bode magnitude plots. (D) Bode phase plots. Note that only the DRT correctly manifests the order of water contents via the location of the second peak.

5.2.1. Fruit ripening

Figure 4A displays the DRT of the collected mandarin ripening (MR) measurements from Chowdhury *et al.* [6] where the authors considered an EEC consisting of a resistor serially connected to a parallelly connected CPE and resistor (with similar impedimetric behaviour as a ZARC element). Two peaks are observed for all stages of ripeness. The first peak's amplitude and relaxation time increase as ripening progresses. A less visually clear trend is the decrease in the relaxation time of the second peak during the ripening of the mandarin oranges. After fitting and evaluating the linear regression models described in Section 5.2, the most suitable model to describe mandarin ripening turned out to be Eq 16, resulting in:

$$R_{\text{days}}(\gamma(\tau_{\text{peak}_1})) = -2.22 + 0.0011\gamma(\tau_{\text{peak}_1}), \tag{19}$$

where R_{days} is the days of ripening and $\gamma(\tau_{\text{peak}_1})$ is the amplitude of the first peak in the DRT. The linear fit and the original observations are displayed in Figure 4A and B. The linear regression fit yielded a coefficient of determination $R^2 = 0.960$. When evaluating the predictive performance using LOOCV, an R^2 value of 0.926 is attained using Eq. (18). The resulting model is given by:

$$R_{\text{days,predict}}(\tau_{\text{peak}_1}), \gamma(\tau_{\text{peak}_1})) = -2.33 + 1.17\tau_{\text{peak}_1} + 2.38\log_{10}\gamma(\tau_{\text{peak}_1}). \tag{20}$$

The persimmon ripening EIS measurements conducted by Harker and Forbes [39] were originally analysed using the double shell model (see Figure 2C). We can see from Figure 4C that the impedance initially increases between 1 and 21 days, as was the case with the ripening of mandarin oranges. The DRT plot also shows a similar pattern as for the mandarin orange between 1 and 21 days, where the two peaks of the DRT move to higher relaxation times. After 35 days, an opposite phenomenon is observed.

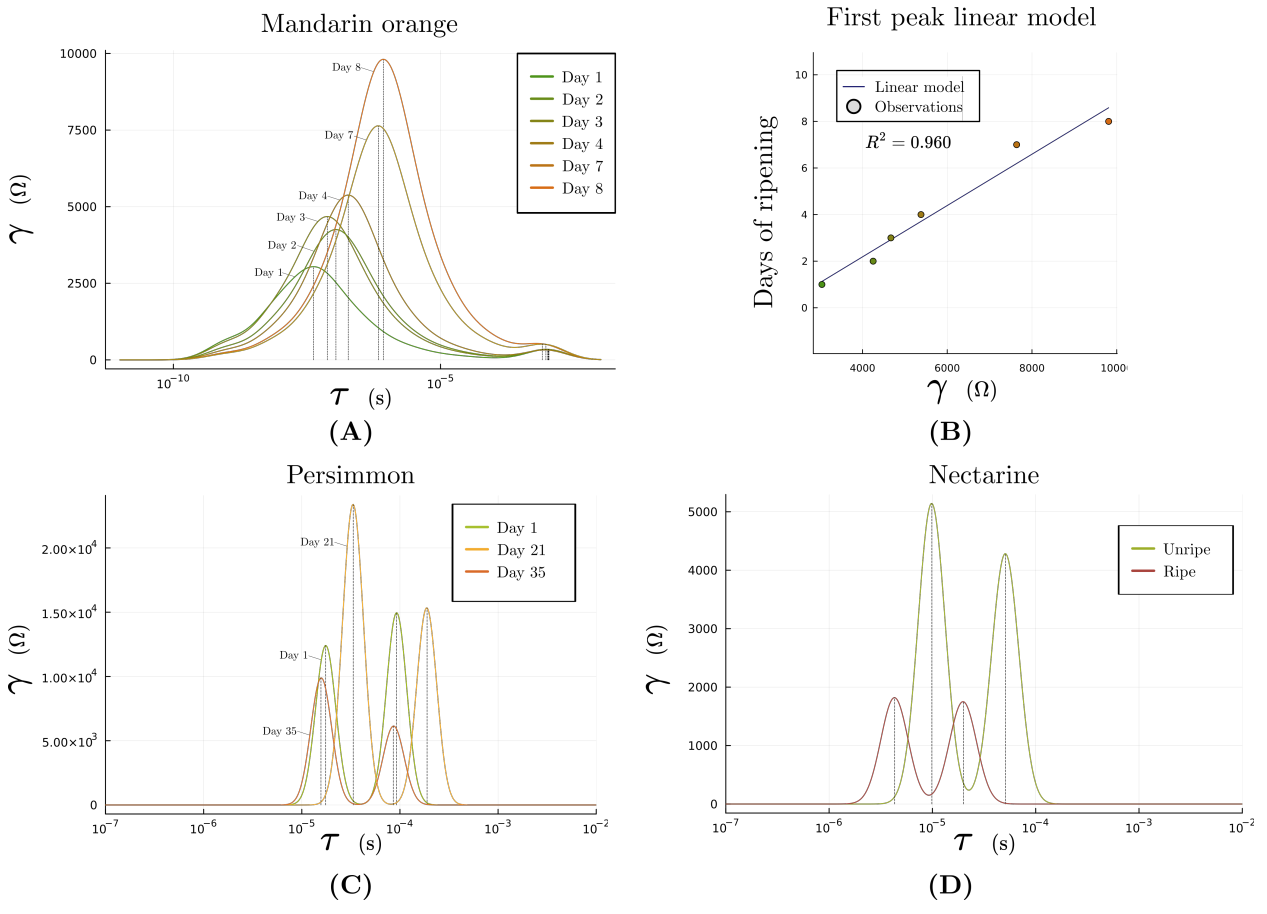

Figure 4: Impedimetric analysis of fruit ripening using DRT analysis. (A) DRT of mandarin orange during 6 days of ripening and (B) the results of a linear regression fit using τ_{peak_1} and $\gamma(\tau_{peak_1})$. (C) Ripening of persimmon fruit. (D) Nectarine ripening.

Figure 4D displays the DRT of measurements from Harker *et al.*'s double shell EEC model-based nectarine ripening analysis [40], where we observe a decrease in the impedance and a shift to lower relaxation times after ripening. These results resemble what happens during the final stages of persimmon ripening between 21 and 35 days.

5.2.2. Abiotic stress

Figure 5 displays the DRTs calculated from Zhang and Willison's carrot freeze-thaw injury measurements. As the authors reported the equivalent circuit parameter values for the double shell and the single shell model, we can compare the two, allowing us to demonstrate the bias introduced by the choice of the equivalent circuit configuration during EIS analysis. From the quality of the complex non-linear least squares (CNLS) fit, the authors recognised that the single shell model was not as capable of modelling the EIS measurements as the double shell model. Figure 5A shows the corresponding DRTs. Freezing at -3 or -6°C manifests itself as a decrease in impedance magnitude and shift to lower relaxation times of both peaks. At -9°C, the freeze damage causes one of the peaks to disappear, as well as a further decrease in impedance magnitude. Figure 5B shows the same analysis conducted based on the assumption of the single shell model. Here, the DRTs all consist of a single peak, and the -3 and -6°C freeze-thawed carrot tissues become indistinguishable. In both cases, the impedance magnitude of the -12°C freeze treatments becomes negligible compared to the earlier treatments. The authors reported a considerably improved fit of the double shell model, which is also reflected in the increased information to be seen in the corresponding DRT. This is not always the case, as some works report an excellent fit with the single shell model (i.e., homogeneous tissues where only a single polarisation process is of significance).

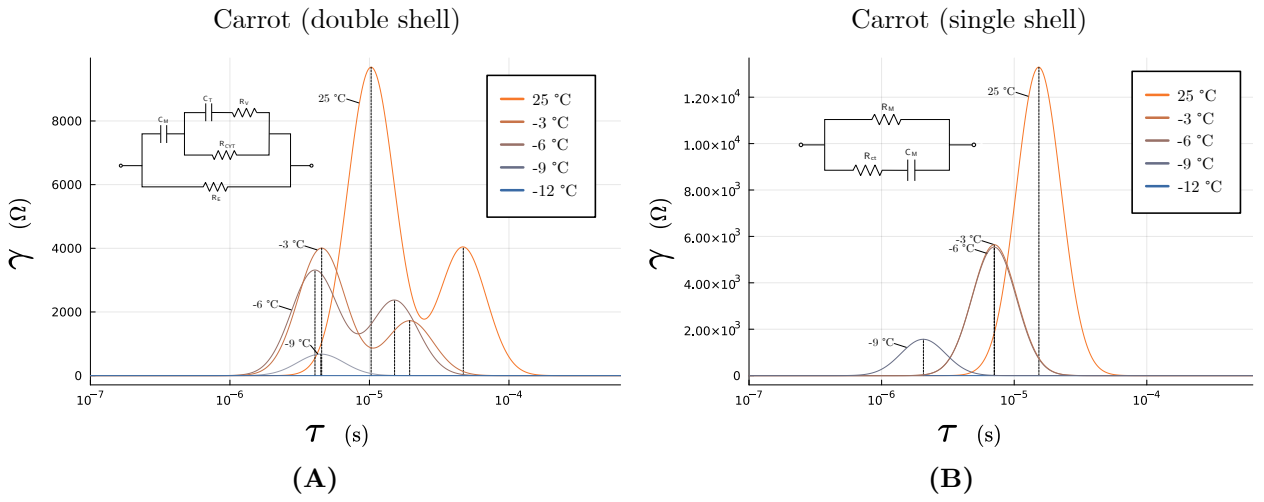

Figure 5: Influence of freezing on the DRT of carrot root cortical tissue. The DRT of impedance measurements simulated using the reported parameters of the double shell model is displayed in (A), whereas that of the single shell model is shown in (B), illustrating how an excessively simple equivalent circuit model can introduce bias into the analysis of EIS measurements.

The DRTs of Watanabe *et al.*'s experiments impedimetrically evaluating mechanical damage of Japanese pears (JP) [42] are displayed in Figure 6. Here we see a consistent shortening of the relaxation time with increasing damage to the Japanese pear tissue. Furthermore, the gradual decrease in amplitude with increasing damage corroborates the reported decreasing impedance due to membrane ruptures and electrolyte leakage. A linear fit to the damage scores using the relaxation time feature (Eq. (15)) results in the following model:

$$D(\tau_{\text{peak}}) = -2.55 - 2.75\tau_{\text{peak}}\,, \tag{21}$$

where $D(\tau_{\text{peak}})$ is the damage score described in Section 3.2, presented as a function of the relaxation time feature. The fit linear regression model given by Eq. (21) yields an R^2 value of 0.985. The best predictive performance is attained using Eq. (18). This results in the following model:

$$D_{\text{predict}}(\tau_{\text{peak}}, \gamma\tau_{\text{peak}}) = -42.98 + 2.00\tau_{\text{peak}} - 9.37\log_{10}\gamma\tau_{\text{peak}}\,, \tag{22}$$

which has a LOOCV R^2 predictive performance value of 0.960 with only a limited number of measurements.

5.2.3. Seed germination

A Voigt model consisting of a resistor and two ZARC elements (i.e., Figure 2A with $N = 2$) was used in the studies of bean seed impedance spectroscopy by Paine *et al.* [47] and Repo *et al.* [48]. Figure 7 displays the DRTs of the snap beans for different moisture contents. The decrease in the impedance of both relaxation processes can be seen with increasing moisture content. In this case, higher moisture leads to greater ion mobility which, in turn, decreases the impedance. Differences in relaxation times can be observed for different moisture contents and between seed viabilities at a given moisture content. According to the authors of these studies, this first relaxation process is due to the cell membranes, while the second relaxation process is due to the cell walls.

Next, we consider snap and soybean EIS measurements conducted by Vozary *et al.* [49]. These were analysed with an EEC containing 3 ZARC elements (see Figure 2A with $N = 3$). When comparing the DRTs displayed in Figure 8 to the dispersion arcs in the Nyquist representations reported in the original publication [49], one can see that the DRTs provide an improved resolution of the different polarisation processes which, in itself, provides sufficient motivation to adopt the DRT analysis method. Based on the investigations by Kuang and Nelson [62], the first peaks (relating to the higher frequencies) are assumed to be caused by the plasmalemma of cellular membranes, while the second peaks (at lower frequencies) are assumed to be caused by the cell walls. The peaks at the lowest frequencies are assumed to be due to the embryo and the space between the two cotyledons. The disappearance of this DRT peak in non-viable seeds

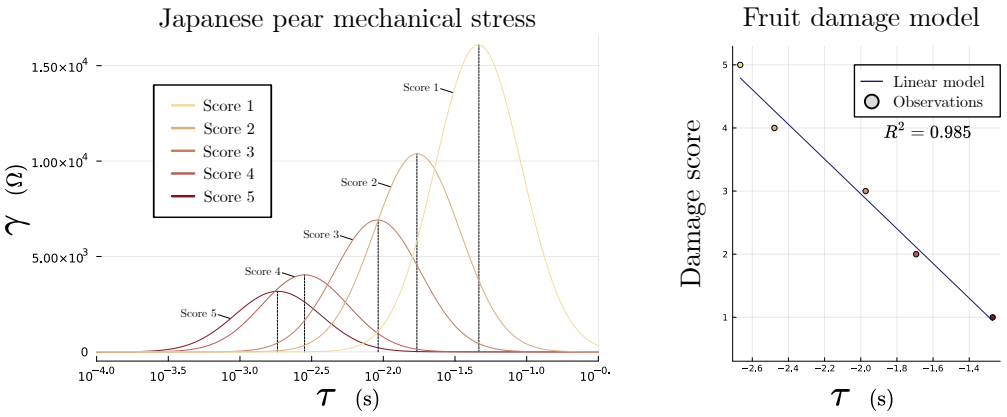

Figure 6: Mechanical damage to fruit. The DRTs of the pears subjected to increasing degrees of drop shock damage (left). The linear regression model using the relaxation times τ, given by Eq. (21), is capable of describing the extent of damage to the fruit (right).

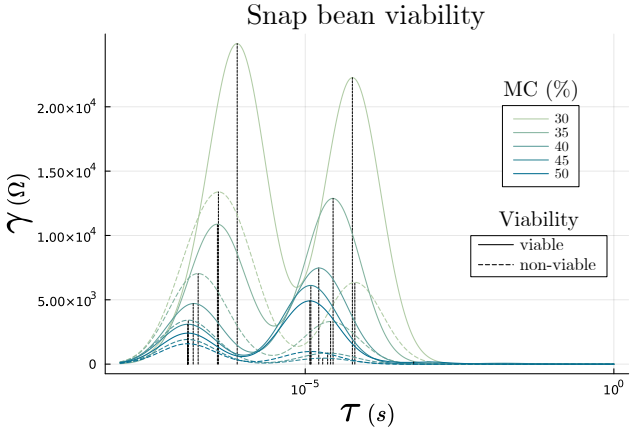

Figure 7: DRTs of snap beans of different Moisture Content (MC) and physiological condition (viable vs non-viable) measured at longitudinal positions.

is assumed to be caused by membrane injury of embryonic tissue and characteristic changes in the inter-cotyledon space. Due to the ventral location of the embryos in the seeds, this peak is less pronounced for the measurements at the longitudinal position, where it is not present for snap beans.

5.2.4. Plant nutrition

Impedimetric analyses by Meiqing *et al.* [4, 51] and Jinyang *et al.* [52] evaluated the N, P, and K status of tomato plants[1] employing a similar methodology with EEC analysis using the fractional single shell model (see Figure 2B) and step-wise linear model selection of impedance measurement values to find the optimal variables for their linear models. The variables to select from were impedance moduli and capacitance values at a range of frequencies. The reported coefficients of determination (R^2) were 0.837, 0.864, and 0.856 for the respective N, P, and K regression models. In the present work, linear regression models were fitted using the relaxation times τ and their corresponding amplitudes $\gamma(\tau)$. Among the models presented in Eqs. 15–18, the most suitable models for the determination of the N, P, and K concentration of tomato plants turned out to be Eqs. 16, 17, and 16, respectively. Fitting these linear regressions results in the following equations:

$$C_{N\%}(\gamma(\tau_{\text{peak}})) = 1.09 + 4.25e - 5\gamma(\tau_{\text{peak}}), \tag{23}$$

$$C_{P\%}(\tau, \gamma(\tau_{\text{peak}})) = 4.42 + 0.79\tau_{\text{peak}} + -6.69e - 6\gamma(\tau_{\text{peak}}), \tag{24}$$

[1] abbreviated below as TPN, TPP, and TPK, respectively.

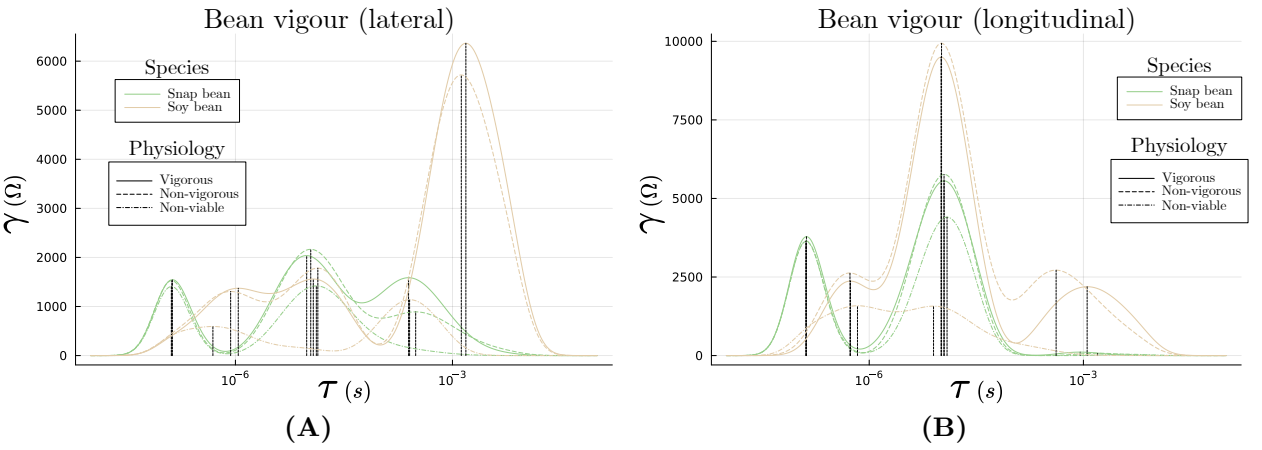

Figure 8: DRTs of snap beans and soybeans in different physiological conditions measured at longitudinal and lateral positions.

$$C_{K\%}(\gamma(\tau_{\text{peak}})) = 2.12 + 1.52e - 5\gamma(\tau_{\text{peak}})\,. \tag{25}$$

Here, $C_{\%}$ denotes the concentration of the considered nutrient. The DRTs and fitted linear models are displayed for the three considered nutrients in Figure 9A, B, and C, respectively. Note that the bivariate linear model for phosphorus is shown in only two dimensions, which is why it is not a straight line such as linear models for the other two nutrients. The best-performing linear regression models for the prediction of nitrogen content and potassium content are the same as those for inference, namely Eqs. (24) and (25). Equation (18) yields the best LOOCV R^2 value for the prediction of the phosphorus content and yields the following model:

$$C_{P\%,\text{predict}}(\tau, \gamma(\tau_{\text{peak}})) = 8.48 + 0.89\tau_{\text{peak}} - 0.84\log_{10}\gamma(\tau_{\text{peak}})\,, \tag{26}$$

The linear regression models evaluated using LOOCV result in R^2 values of 0.917, 0.836, and 0.951 for the N, P, and K regression models. While these and previous results show that NPK deficiency can be detected using EIS when all other nutrient values are kept constant, further research is required to evaluate whether deficiencies in one of these nutrients can be ascertained while the others are also variable.

5.2.5. Processing of plant products

Figure 10A (left) presents the DRTs of the measured potato samples for the different heat treatment regimes applied by Imaizumi *et al.* [53]. A clear trend is the decreased impedance as the heat treatments intensify. There is also a clear shortening of the distribution times, which was used to fit a linear regression model demonstrating their capability to model the change in the texture and softness (quantified by the internal penetration force (PF) reported as F_{I} by the authors) of the considered food product after the blanching treatments. This linear model given by Eq. (15) is the most suitable among the four evaluated DRT-based linear regression models. The resulting fitted linear model is displayed on the right-hand side of Figure 10A and is expressed as:

$$F_{\text{I}}(\tau) = 32.42 + 4.67\tau\,. \tag{27}$$

The best LOOCV R^2 performance value of 0.840 was achieved using Eq. (18) for the fit of Eq. (27). As such we obtain the following fitted model:

$$F_{\text{I,predict}}(\tau) = -64.60 - 7.49\tau + 9.51\log_{10}\gamma(\tau)\,. \tag{28}$$

The same authors [63] applied hot water treatment over a range of temperatures to *Ipomoea batatas* L. (sweet potato) and subsequently evaluated changes in tissue structure, moisture content, porosity, mechanical, and electrical properties of the tubers in parallel with fitting the parameters of the fractional single shell model. The latter was done using EIS. A similar effect of the various heat treatments on the DRTs as the previous investigation can be seen on the left in

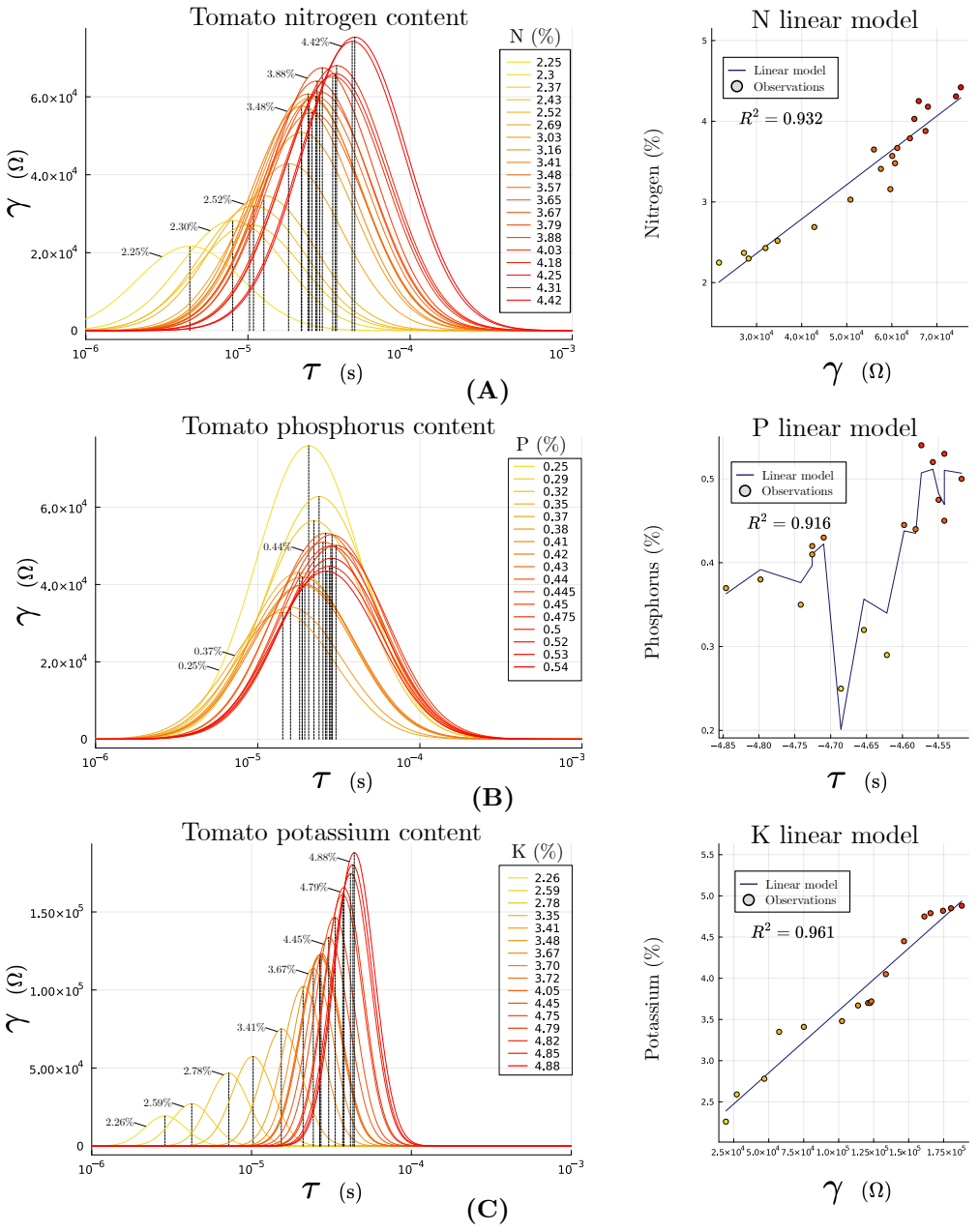

Figure 9: The nutritional NPK status of tomato plants is reflected in their DRTs. (A), (B) and (C) display the DRT for varying potassium, phosphorus, and nitrogen concentrations. The DRT figures are accompanied by visualizations of the fitted linear models given by Eqs. (24)–(25) using the DRT-based features. The reported coefficients of determination R^2 in this figure illustrate the capacity of the linear models to describe the nutrient concentration of tomato plants.

Figure 10B. A linear model based on the relaxation times and their amplitudes for the porosity or void fraction (VF) can be seen on the right side of Figure 10B and yields a R^2 value of 0.956. This also yields the most performant predictive model with a LOOCV R^2 value of 0.950:

$$P(\tau_{\text{peak}}, \gamma(\tau_{\text{peak}_1})) = 0.79 + 0.11\tau_{\text{peak}} + 6.48e-5\gamma(\tau_{\text{peak}})\,. \tag{29}$$

Table 1
Summary of the most suitable evaluated DRT-based linear regression models from the considered applications in plant agriculture: mandarin ripening (MR), Japanese pear mechanical stress (JP), tomato plant nitrogen content (TPN), tomato plant phosphorus content (TPP), tomato plant potassium content (TPK), penetration force of heat-treated potatoes (PF), porosity or void fraction of heat-treated sweet potatoes (VF), and fractional stress of blanched spinach (FS).

Experiment	Var.	Coefficient	95% Conf. Int.	Std. Error	t	Pr(> $\lvert t \rvert$)	R^2
MR	Intercept	-2.22	[-4.00,-0.43]	0.64	-3.46	0.025	0.960
	$\gamma(\tau_{\text{peak}_1})$	1.10e-3	[0.81e-3,1.30e-3]	1.0e-4	10.68	0.0004	
JP	Intercept	-2.55	[-3.84,-1.27]	0.402	-6.34	0.0079	0.985
	τ_{peak_1}	-2.75	[-3.37,-2.13]	0.194	-14.22	0.0008	
TPN	Intercept	1.09	[0.77,1.41]	0.152	7.17	<1e-05	0.932
	$\gamma(\tau_{\text{peak}_1})$	4.25e-5	[3.68e-5,4.82e-5]	2.70e-6	15.71	<1e-11	
TPP	Intercept	4.42	[-26.12,54.11]	0.351	12.62	<1e-08	0.916
	τ_{peak_1}	0.79	[-3.04,7.17]	7.22e-2	10.98	<1e-07	
	$\gamma(\tau_{\text{peak}_1})$	-6.69e-6	[-4.0e-4, 2.0e-3]	6.79e-7	-9.84	<1e-06	
TPK	Intercept	2.12	[1.91,2.33]	0.099	21.47	<1e-11	0.961
	$\gamma(\tau_{\text{peak}_1})$	1.52e-5	[1.35e-5,1.69e-5]	7.90e-7	19.20	<1e-11	
PF	Intercept	32.42	[28.21,36.63]	2.03	15.98	<1e-12	0.859
	τ_{peak_1}	4.67	[3.83,5.51]	0.404	11.55	<1e-10	
VF	Intercept	0.794	[0.516,1.073]	0.138	5.78	<1e-05	0.956
	τ_{peak_1}	0.113	[0.068 ,0.158]	0.0222	5.09	<1e-04	
	$\gamma(\tau_{\text{peak}_1})$	6.48e-5	[5.25e-5,7.72e-5]	6.08e-6	10.67	<1e-12	
FS	Intercept	7.10	[1.64,12.55]	1.71	4.14	0.0256	0.941
	τ_{peak_1}	0.45	[0.001,0.894]	0.14	4.72	0.0497	
	$\log_{10}\gamma(\tau_{\text{peak}_1})$	-1.03	[-1.84,-0.22]	0.254	-4.06	0.0270	

The calculated DRTs for investigations by Watanabe *et al.* [54] utilising impedance spectroscopy with fractional single shell EEC model parameter fitting after heat treatments of spinach also show a similar shortening of the relaxation time and a decrease in the impedance magnitudes. This can be seen in Figure 10C, along with the linear model based on the DRTs to fit the fracture stress (FS) with $R^2 = 0.941$ and a LOOCV R^2 value of 0.854. The fracture stress is a mechanical property of the food specimens, calculated as the ratio of the maximum load to the cross-sectional area.

$$S(\tau_{\text{peak}_1}, \gamma(\tau_{\text{peak}_1})) = 7.10 + 0.45\tau_{\text{peak}_1} - 1.03\log_{10}\gamma(\tau_{\text{peak}_1}), \tag{30}$$

where $S(\tau_{\text{peak}_1}, \gamma(\tau_{\text{peak}_1}))$ denotes the fracture stress as a function of the relaxation times and amplitudes of the DRT peaks.

5.2.6. Summary of regression model estimates

Table 1 summarises the best-performing linear regression model estimates, their confidence intervals, standard errors and significance. Table 2 compares the LOOCV-based predictive performances of the four considered DRT-based regression models (Eqs. (15)–(18)) using their R^2 values. One can observe that for experiments considering the tomato plant nitrogen content, tomato plant potassium content, sweet potato porosity and spinach fractional stress experiments the regression models for inference also yield the best predictive performances. This is not the case for the mandarin ripening, Japanese pear mechanical damage, tomato plant phosphorus, and potato penetration force case studies, where Eq. (18) yields the best-performing linear models for prediction given by Eqs. (20), (22), (26), and (28), respectively. For all the considered case studies, we can observe in Table 2 that one or more of the considered DRT-based linear regression models are capable of adequately predicting the property of interest.

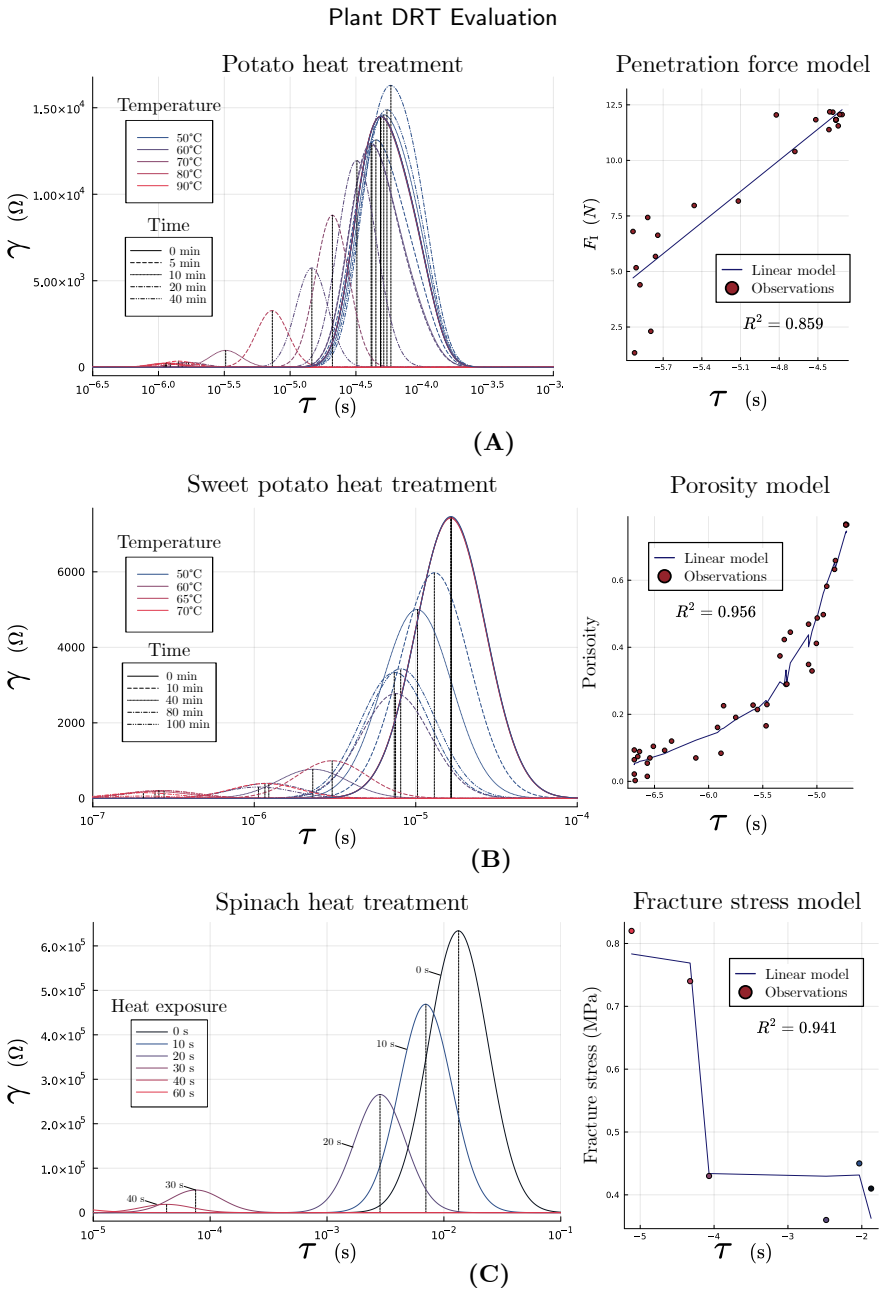

Figure 10: Heat treatment of vegetables. (A) DRT of potato samples subjected to varying heat treatments (left) and the fitted linear model based on the relaxation times to model the internal penetration force of the potato samples at varying heat treatments, given by Eq. (27) (right). (B) DRT representations of heat-treated sweet potato samples (left) and the linear model based on DRT features to model the porosity of the heat-treated samples, given by Eq. (29) (right). (C) DRT of heat-treated spinach samples (left) and the linear model based on DRT features to model the fracture stress of the samples using DRT features, given by Eq. (30) (right).

6. Accompanying software

The publicly available software developed for this work is a Julia package called `DRT.jl`. It uses a radial-basis-function-based discretisation, followed by Tikhonov regularisation to calculate the distribution of relaxation times of impedance spectra. The software together with documentation and examples can be found at `https://github.com/MaximeVH/DRT.jl`.

Table 2
LOOCV R^2 values for the four considered DRT-based linear regression models predicting plant (product) properties. Models 1–4 represent Eqs. (15)–(18).

Experiment	Model 1	Model 2	Model 3	Model 4
MR	0.903	0.864	0.791	**0.926**
JP	0.956	0.679	0.911	**0.960**
TPN	0.776	**0.917**	0.870	0.775
TPP	0.197	0.124	0.723	**0.836**
TPK	0.828	**0.951**	0.943	0.832
PF	0.822	0.680	0.821	**0.840**
VF	0.803	0.921	**0.950**	0.877
FS	0.327	0.160	0.276	**0.854**

7. Discussion

A limitation of the current work is the reliance on impedance spectroscopy data reported in the literature, which are currently limited in quality and quantity. The further development of novel methods for analysing impedance spectroscopy measurements for plant applications would greatly benefit from publishing and maintaining collected data in a public database accessible to other researchers. This could be done in a fashion similar to the many databases available for the bio-informatics community, such as Uniprot [64] and Genbank [65], to name a few.

Ehosioke *et al.* [66] stated that future EIS-based studies analyzing root systems should incorporate the microscopic level interpretations, which are based on the roots' physiological properties so as to improve the understanding of the polarization mechanisms at the root segment scale. We envision that the DRT-based analysis of EIS measurements will make such interpretations possible. The same goes for the interpretation of multi-component system measurements.

Equivalent circuit models need to be chosen on a case-by-case basis, and different equivalent electrical circuits are being proposed for different fruit varieties [6]. Additionally, mathematical models are being proposed that use a selection of the measured impedance measurements to predict plant properties (e.g., selected using backward elimination [51]). These observations show that there is no generally applicable model for a specific physiological plant feature. The DRT method uses all the information in the EIS measurements, and it provides generally applicable predictive features.

The number of measurements in EIS studies is typically in the range of tens to a few hundred, highlighting the need for informative features to achieve optimal predictive performance. Even in cases where a large number of measurements is available, sophisticated deep learning models can be supplemented with additional informative features such as EEC parameters and DRT features using multimodal data fusion methods for further improvement [67, 68].

A commonly reported weakness of EIS is its ambiguous and system-dependent interpretation. A thorough experimental characterisation of application-specific DRTs will be a step toward mitigating this issue. As a novel analysis method, DRT analysis is not exempt from due criticism. Much work has yet to be done on the rigorous interpretation of the DRT for plant systems. Furthermore, analyzing experimental impedance measurements with the DRT requires high data quality standards to be met and a sufficiently high frequency resolution (i.e., many measurements over the relevant frequency range) to be used in order to obtain clear and reproducible results. Before calculating the DRT, we recommend the evaluation of the validity of EIS measurements using the Kramers–Kronig relations or their modern variants [33].

While there is tremendous potential for the adoption of the DRT analysis method for the characterisation of plant systems, a drawback is that it requires many (around 100) high-quality EIS measurements over the relevant frequency range without the measurement taking long enough for the linearity requirement of EIS to no longer be applicable. Furthermore, its computational cost is larger than a quick CNLS fit of (a part of) an impedance spectrum, resulting in a larger hardware burden for in-field applications. However, these issues are being resolved with the rapid progress of microcontroller systems. Plant applications of EIS with around 100 measurements within the frequency range of interest are already common in recent work [69].

Ivers–Tiffee and Weber [16] report two main uses of the DRT analysis method: (i) The black box approach, where no physicochemical background is required. In this approach, the goal is to predict the considered system's dynamic behaviour. (ii) The rigorous identification of the different processes in a complex electrochemical system. The former

approach is mainly considered in this work, where we found that features provided by the DRT analysis method are very useful in modelling the physiological properties of plants. While some indications of the underlying interpretation of the relaxation times can be ascertained from the relevant literature [62, 70], rigorous studies investigating the DRT based on many high-quality measurements and over different experimental conditions are required to fully characterise the biological meaning of the DRT peaks. This has also been the case for the in-depth characterisation of fuel cells and Li-ion batteries using the DRT analysis method [71, 72].

Obtaining a DRT using Tikhonov regularisation [73] at present requires some fine-tuning of the regularisation hyper-parameter, and according to Ivers–Tiffee and Weber [16], this step is unlikely to be robustly automated. Another reported weakness of the DRT analysis method is that it is not good at dealing with inductive effects. However, this is not an issue for the analysis of biological tissues, as they show capacitive rather than inductive behaviour [74].

The simulations based on equivalent electrical circuits used in this work are according to the previous authors' choice of equivalent electrical circuit model, which can be subject to bias [75]. The simulations are also limited to the previous authors' number and quality of measurements within the frequency range. The case studies give an indication of the effectiveness of the DRT analysis method. Nevertheless, due to the simulation-based nature of this study, with the simulated spectra limited by the capacity of the underlying circuit models, the potential of the DRT analysis method is likely to be far greater than presented in this work. In spite of these limitations, a high predictive performance is already achieved through use of the DRT features in the considered case studies in Section 5.2. From Tables 1 and 2 one can observe that relaxation times or their corresponding amplitudes by themselves are often adequate for describing changes in plant physiology, with models containing both typically performing best for prediction. Therefore, the collection of impedance measurements of sufficiently high frequency resolution impedance measurements of plant systems in varying physiological states, followed by a DRT analysis, is the next step to be undertaken in future work. High-quality measurements will be required to optimally capture the electrochemical information that can be interrogated from the plant systems through EIS, which will be reflected in the DRTs and provide more detailed information on the electrochemical processes taking place during fruit ripening and other plant applications of interest.

Besides the case studies discussed in the present work, many other applications of plant impedance spectroscopy (e.g., in agriculture) can benefit from DRT analysis. These include fruit ripeness and quality control [76, 77, 78], drought stress [79], morphological damage [80, 81], irradiation [1], frost hardness [82, 83, 84, 85], chemical damage [86], nutrient status [51, 87], and infectious diseases [88, 89], to name but a few.

8. Conclusion and future perspectives

A great deal of information on the physiological status of plants is contained in their electrochemical impedance spectra. One of the main challenges for plant EIS practitioners is extracting this information. In this work, we conducted the first thorough simulation-based evaluation of the emerging Distribution of Relaxation Times analysis method in plant EIS applications. With a sufficient number of high-quality measurements, the distribution of relaxation times would provide informative features for predictive models able to classify the physiological status of plants and their fruits.

The simulation-based case studies in this work demonstrate that the DRT analysis method holds promise for the investigation of a range of plant properties, yet there is still much to explore for unravelling the full potential of this method. These results, along with recent studies on other biological systems and the freely available software developed software in this work, give the impetus for further work on analysing plant systems on the basis of DRTs. High-quality impedance measurements of different plant organs with a sufficiently high frequency resolution will allow practitioners to obtain an impedimetric fingerprint of a plant's physiological status, as is the case for fuel cells, where DRT-based EIS investigations are already becoming common practice.

Author statement

Maxime Van Haeverbeke: conceptualization, methodology, software, formal analysis, visualization, writing - original draft, validation. **Bernard De Baets**: conceptualization, writing - editing, supervision. **Michiel Stock**: conceptualization, writing - editing, supervision.

Declaration of competing interest

The authors declare that they have no known competing financial interests or personal relationships that could have appeared to influence the work reported in this paper.

Acknowledgements

This work was supported by FWO-Vlaanderen under grant FWO-SBO S007019N (Bisceps).

References

[1] Felföldi, J., László, P., Barabássy, S., and Farkas, J. Dielectric method for detection of irradiation treatment of potatoes. *Radiation Physics and Chemistry*, 41(3):471–480, 1993.

[2] Hamed, K. B., Zorrig, W., and Hamzaoui, A. H. Electrical impedance spectroscopy: A tool to investigate the responses of one halophyte to different growth and stress conditions. *Computers and Electronics in Agriculture*, 123:376–383, 2016.

[3] Tomkiewicz, D. and Piskier, T. A plant based sensing method for nutrition stress monitoring. *Precision Agriculture*, 13(3):370–383, 2012.

[4] Meiqing, L., Jinyang, L., Xinhua, W., and Wenjing, Z. Early diagnosis and monitoring of nitrogen nutrition stress in tomato leaves using electrical impedance spectroscopy. *International Journal of Agricultural and Biological Engineering*, 10(3):194–205, 2017.

[5] Ibba, P., Falco, A., Abera, B. D., Cantarella, G., Petti, L., and Lugli, P. Bio-impedance and circuit parameters: An analysis for tracking fruit ripening. *Postharvest Biology and Technology*, 159:110978, 2020.

[6] Chowdhury, A., Singh, P., Bera, T. K., Ghoshal, D., and Chakraborty, B. Electrical impedance spectroscopic study of mandarin orange during ripening. *Journal of Food Measurement and Characterization*, 11(4):1654–1664, 2017.

[7] Lu, Y., Zhao, C.-Z., Huang, J.-Q., and Zhang, Q. The timescale identification decoupling complicated kinetic processes in lithium batteries. *Joule*, 6(6):1172–1198, 2022.

[8] Ciucci, F. Modeling electrochemical impedance spectroscopy. *Current Opinion in Electrochemistry*, 13:132–139, 2019.

[9] Ramírez-Chavarría, R. G., Sánchez-Pérez, C., and Matatagui, D. Analysis of impedance spectroscopy measurements of biological tissue using the distribution of relaxation times method. In *Proceedings of the 10th International Joint Conference on Biomedical Engineering Systems and Technologies (BIOSTEC 2017) - BIODEVICES*, volume 1, pages 224–228. INSTICC, SciTePress, 2017.

[10] Ramírez-Chavarría, R., Sánchez-Pérez, C., Matatagui, D., Qureshi, N., Pérez-García, A., and Hernández-Ruíz, J. Ex-vivo biological tissue differentiation by the distribution of relaxation times method applied to electrical impedance spectroscopy. *Electrochimica Acta*, 276:214–222, 2018.

[11] Ramírez-Chavarría, R. G., Sánchez-Pérez, C., Romero-Ornelas, L., and Ramón-Gallegos, E. Time-constant-domain spectroscopy: an impedance-based method for sensing biological cells in suspension. *IEEE Sensors Journal*, 21(1):185–192, 2020.

[12] Shi, F. and Kolb, J. F. Enhanced resolution impedimetric analysis of cell responses from the distribution of relaxation times. *Biosensors and Bioelectronics*, 157:112149, 2020.

[13] Wang, H., Long, X., Sun, Y., Wang, D., Wang, Z., Meng, H., Jiang, C., Dong, W., and Lu, N. Electrochemical impedance spectroscopy applied to microbial fuel cells: A review. *Frontiers in Microbiology*, 13:973501, 2022.

[14] Feldman, Y., Puzenko, A., and Ryabov, Y. Dielectric relaxation phenomena in complex materials. In Coffey, W. and Kalmykov, Y., editors, *Fractals, Diffusion, and Relaxation in Disordered Complex Systems*, volume 133 of *Advances in Chemical Physics*, pages 1–125. John Wiley & Sons, Inc., Hoboken, NJ, USA, 2006.

[15] Schichlein, H., Müller, A. C., Voigts, M., Krügel, A., and Ivers-Tiffée, E. Deconvolution of electrochemical impedance spectra for the identification of electrode reaction mechanisms in solid oxide fuel cells. *Journal of Applied Electrochemistry*, 32:875–882, 2002.

[16] Ivers-Tiffee, E. and Weber, A. Evaluation of electrochemical impedance spectra by the distribution of relaxation times. *Journal of the Ceramic Society of Japan*, 125(4):193–201, 2017.

[17] Boukamp, B. A. Distribution (function) of relaxation times, successor to complex nonlinear least squares analysis of electrochemical impedance spectroscopy? *Journal of Physics: Energy*, 2(4):042001, 2020.

[18] Leonide, A., Sonn, V., Weber, A., and Ivers-Tiffée, E. Evaluation and modeling of the cell resistance in anode-supported solid oxide fuel cells. *Journal of the Electrochemical Society*, 155(1):B36–B41, 2007.

[19] Dierickx, S., Weber, A., and Ivers-Tiffée, E. How the distribution of relaxation times enhances complex equivalent circuit models for fuel cells. *Electrochimica Acta*, 355:136764, 2020.

[20] Iurilli, P., Brivio, C., Carrillo, R. E., and Wood, V. Eis2mod: A drt-based modeling framework for li-ion cells. *IEEE Transactions on Industry Applications*, 58(2):1429–1439, 2021.

[21] Wildfeuer, L., Gieler, P., and Karger, A. Combining the distribution of relaxation times from eis and time-domain data for parameterizing equivalent circuit models of lithium-ion batteries. *Batteries*, 7(3):52, 2021.

[22] Tuncer, E. and Gubanski, S. On dielectric data analysis. using the monte carlo method to obtain relaxation time distribution and comparing non-linear spectral function fits. *IEEE Transactions on Dielectrics and Electrical Insulation*, 8(3):310–320, 2001.

[23] Hershkovitz, S., Tomer, S., Baltianski, S., and Tsur, Y. ISGP: Impedance spectroscopy analysis using evolutionary programming procedure. *ECS Transactions*, 33(40):67, 2011.

[24] Boukamp, B. A. Fourier transform distribution function of relaxation times; application and limitations. *Electrochimica Acta*, 154:35–46, 2015.

[25] Macutkevic, J., Banys, J., and Matulis, A. Determination of the distribution of the relaxation times from dielectric spectra. *Nonlinear Analysis: Modelling and Control*, 9(1):75–88, 2004.

[26] Effat, M. B. and Ciucci, F. Bayesian and hierarchical bayesian based regularization for deconvolving the distribution of relaxation times from electrochemical impedance spectroscopy data. *Electrochimica Acta*, 247:1117–1129, 2017.

[27] Quattrocchi, E., Wan, T. H., Belotti, A., Kim, D., Pepe, S., Kalinin, S. V., Ahmadi, M., and Ciucci, F. The deep-DRT: A deep neural network approach to deconvolve the distribution of relaxation times from multidimensional electrochemical impedance spectroscopy data. *Electrochimica Acta*, 392:139010, 2021.

[28] Wan, T. H., Saccoccio, M., Chen, C., and Ciucci, F. Influence of the discretization methods on the distribution of relaxation times deconvolution: implementing radial basis functions with drttools. *Electrochimica Acta*, 184:483–499, 2015.

[29] Bezanson, J., Edelman, A., Karpinski, S., and Shah, V. B. Julia: A fresh approach to numerical computing. *SIAM Review*, 59(1):65–98, 2017.

[30] Laurie, D. Calculation of Gauss-Kronrod quadrature rules. *Mathematics of Computation*, 66(219):1133–1145, 1997.

[31] Hahn, M., Schindler, S., Triebs, L.-C., and Danzer, M. A. Optimized process parameters for a reproducible distribution of relaxation times analysis of electrochemical systems. *Batteries*, 5(2):43, 2019.

[32] Broyden, C. G. The convergence of a class of double-rank minimization algorithms: 2. The new algorithm. *IMA Journal of Applied Mathematics*, 6(3):222–231, 1970.

[33] Schönleber, M., Klotz, D., and Ivers-Tiffée, E. A method for improving the robustness of linear Kramers-Kronig validity tests. *Electrochimica Acta*, 131:20–27, 2014.

[34] Saccoccio, M., Wan, T. H., Chen, C., and Ciucci, F. Optimal regularization in distribution of relaxation times applied to electrochemical impedance spectroscopy: ridge and lasso regression methods-a theoretical and experimental study. *Electrochimica Acta*, 147:470–482, 2014.

[35] Choi, M.-B., Shin, J., Ji, H.-I., Kim, H., Son, J.-W., Lee, J.-H., Kim, B.-K., Lee, H.-W., and Yoon, K. J. Interpretation of impedance spectra of solid oxide fuel cells: L-curve criterion for determination of regularization parameter in distribution function of relaxation times technique. *Jom*, 71:3825–3834, 2019.

[36] Paul, T., Chi, P., Wu, P. M., and Wu, M. Computation of distribution of relaxation times by tikhonov regularization for Li-ion batteries: usage of l-curve method. *Scientific Reports*, 11(1):12624, 2021.

[37] Maradesa, A., Py, B., Wan, T. H., Effat, M. B., and Ciucci, F. Selecting the regularization parameter in the distribution of relaxation times. *Journal of The Electrochemical Society*, 170(3):030502, 2023.

[38] Van Haeverbeke, M., De Baets, B., and Stock, M. Plant impedance spectroscopy: a review of modeling approaches and applications. *Frontiers in Plant Science*, 14(1187573), 2023.

[39] Harker, F. R. and Forbes, S. K. Ripening and development of chilling injury in persimmon fruit: an electrical impedance study. *New Zealand Journal of Crop and Horticultural Science*, 25(2):149–157, 1997.

[40] Harker, F. R. and Maindonald, J. H. Ripening of nectarine fruit (changes in the cell wall, vacuole, and membranes detected using electrical impedance measurements). *Plant Physiology*, 106(1):165–171, 1994.

[41] Zhang, M. and Willison, J. Electrical impedance analysis in plant tissues: the effect of freeze-thaw injury on the electrical properties of potato tuber and carrot root tissues. *Canadian Journal of Plant Science*, 72(2):545–553, 1992.

[42] Watanabe, T., Nakamura, N., Ando, Y., Kaneta, T., Kitazawa, H., and Shiina, T. Application and simplification of cell-based equivalent circuit model analysis of electrical impedance for assessment of drop shock bruising in japanese pear tissues. *Food and Bioprocess Technology*, 11: 2125–2129, 2018.

[43] Association, I. S. T. et al. ISTA (1996) international rules for seed testing. *Seed Science and Technology*, 21:299–513, 1996.

[44] Lopez Del Egido, L., Navarro-Miró, D., Martinez-Heredia, V., Toorop, P. E., and Iannetta, P. P. A spectrophotometric assay for robust viability testing of seed batches using 2, 3, 5-triphenyl tetrazolium chloride: using hordeum vulgare l. as a model. *Frontiers in Plant Science*, 8:747, 2017.

[45] Jorge, M. H. A. and Ray, D. T. Germination characterization of guayule seed by morphology, mass and, x-ray analysis. *Industrial Crops and Products*, 22(1):59–63, 2005.

[46] Ackmann, J. J. and Seitz, M. A. Methods of complex impedance measurements in biologic tissue. *Critical Reviews in Biomedical Engineering*, 11(4):281–311, 1984.

[47] Paine, D., Repo, T., and Taylor, A. Noninvasive seed quality test by impedance spectrum analysis. *Seed Technology*, 23(2):187–196, 2001.

[48] Repo, T., Paine, D., and Taylor, A. Electrical impedance spectroscopy in relation to seed viability and moisture content in snap bean (phaseolus vulgaris l.). *Seed Science Research*, 12(1):17–29, 2002.

[49] Vozáry, E., Paine, D., Kwiatkowski, J., and Taylor, A. Prediction of soybean and snap bean seed germinability by electrical impedance spectroscopy. *Seed Science and Technology*, 35(1):48–64, 2007.

[50] Kulcheski, F. R., Côrrea, R., Gomes, I. A., de Lima, J. C., and Margis, R. NPK macronutrients and microrna homeostasis. *Frontiers in Plant Science*, 6:451, 2015.

[51] Meiqing, L., Jinyang, L., Hanping, M., and Yanyou, W. Diagnosis and detection of phosphorus nutrition level for solanum lycopersicum based on electrical impedance spectroscopy. *Biosystems Engineering*, 143:108–118, 2016.

[52] Jinyang, L., Meiqing, L., Hanping, M., and Wenjing, Z. Diagnosis of potassium nutrition level in solanum lycopersicum based on electrical impedance. *Biosystems Engineering*, 147:130–138, 2016.

[53] Imaizumi, T., Tanaka, F., Hamanaka, D., Sato, Y., and Uchino, T. Effects of hot water treatment on electrical properties, cell membrane structure and texture of potato tubers. *Journal of Food Engineering*, 162:56–62, 2015.

[54] Watanabe, T., Ando, Y., Orikasa, T., Shiina, T., and Kohyama, K. Effect of short time heating on the mechanical fracture and electrical impedance properties of spinach (Spinacia oleracea L.). *Journal of Food Engineering*, 194:9–14, 2017.

[55] Ozier-Lafontaine, H. and Bajazet, T. Analysis of root growth by impedance spectroscopy (EIS). *Plant and Soil*, 277(1):299–313, 2005.

[56] Van Haeverbeke, M., Stock, M., and De Baets, B. Equivalent electrical circuits and their use across electrochemical impedance spectroscopy application domains. *IEEE Access*, 10:51363–51379, 2022.

[57] Lasia, A. *Electrochemical Impedance Spectroscopy and its Applications*. Springer, New York, 1 edition, 2014.

[58] Macdonald, D. D. and Urquidi-Macdonald, M. Kramers-kronig transformation of constant phase impedances. *Journal of The Electrochemical Society*, 137(2):515, 1990.

[59] Hsu, C. and Mansfeld, F. Concerning the conversion of the constant phase element parameter y0 into a capacitance. *Corrosion*, 57(09), 2001.

[60] Zhang, M. and Willison, J. Electrical impedance analysis in plant tissues8. *Journal of Experimental Botany*, 44(8):1369–1375, 1993.

[61] Zhang, M. and Willison, J. Electrical impedance analysis in plant tissues11. *Journal of Experimental Botany*, 42(11):1465–1475, 1991.

[62] Kuang, W. and Nelson, S. Low-frequency dielectric properties of biological tissues: A review with some new insights. *Transactions of the ASAE*, 41(1):173–184, 1998.

[63] Imaizumi, T., Tanaka, F., Sato, Y., Yoshida, Y., and Uchino, T. Evaluation of electrical and other physical properties of heated sweet potato. *Journal of Food Process Engineering*, 40(3):e12490, 2017.

[64] Apweiler, R., Bairoch, A., Wu, C. H., Barker, W. C., Boeckmann, B., Ferro, S., Gasteiger, E., Huang, H., Lopez, R., Magrane, M., et al. Uniprot: the universal protein knowledgebase. *Nucleic Acids Research*, 32(S1):D115–D119, 2004.

[65] Benson, D. A., Cavanaugh, M., Clark, K., Karsch-Mizrachi, I., Lipman, D. J., Ostell, J., and Sayers, E. W. Genbank. *Nucleic Acids Research*, 41(D1):D36–D42, 2012.

[66] Ehosioke, S., Nguyen, F., Rao, S., Kremer, T., Placencia-Gomez, E., Huisman, J. A., Kemna, A., Javaux, M., and Garré, S. Sensing the electrical properties of roots: A review. *Vadose Zone journal*, 19(1):e20082, 2020.

[67] Ramachandram, D. and Taylor, G. W. Deep multimodal learning: A survey on recent advances and trends. *IEEE Signal Processing Magazine*, 34(6):96–108, 2017.

[68] Stahlschmidt, S. R., Ulfenborg, B., and Synnergren, J. Multimodal deep learning for biomedical data fusion: a review. *Briefings in Bioinformatics*, 23(2):bbab569, 2022.

[69] Arteaga, H., Robleto-Martinez, E., de Sousa Silva, A. C., Souto, S., Batista, J., and Costa, E. J. X. Postharvest freezing process assessment of the blueberry structure in three acts: Bioimpedance, color, and granulometry analysis. *LWT*, 151:112237, 2021.

[70] Foster, K. and Schwan, H. Dielectric-properties of tissues and biological-materials - a critical-review. *Critical Reviews in Biomedical Engineering*, 17(1):25–104, 1989.

[71] Weiß, A., Schindler, S., Galbiati, S., Danzer, M. A., and Zeis, R. Distribution of Relaxation Times Analysis of High-temperature PEM Fuel Cell Impedance Spectra. *Electrochimica Acta*, 230:391–398, 2017.

[72] Zhu, J., Knapp, M., Liu, X., Yan, P., Dai, H., Wei, X., and Ehrenberg, H. Low-temperature separating lithium-ion battery interfacial polarization based on distribution of relaxation times (DRT) of impedance. *IEEE Transactions on Transportation Electrification*, 7(2):410–421, 2020.

[73] Tikhonov, A. N., Goncharsky, A., Stepanov, V., and Yagola, A. G. *Numerical Methods for the Solution of Ill-Posed Problems*, volume 328 of *Mathematics and Its Applications*. Springer, Dordrecht, 1995.

[74] Hussain, M. I., El-Keblawy, A., Akhtar, N., and Elwakil, A. S. Electrical Impedance Spectroscopy in Plant Biology. *Sustainable Agriculture Reviews*, 52:395–416, 2021.

[75] McAdams, E. and Jossinet, J. Problems in equivalent circuit modelling of the electrical properties of biological tissues. *Bioelectrochemistry and Bioenergetics*, 40(2):147–152, 1996.

[76] Mane, N. and Mudhalwadkar, R. Banana ripeness assessment by impedance spectroscopy. In *IEEE International Conference on Power, Control, Signals and Instrumentation Engineering (ICPCSI)*, pages 527–529, Thandalam, India, 2017. IEEE.

[77] Ibba, P., Falco, A., Rivadeneyra, A., and Lugli, P. Low-cost bio-impedance analysis system for the evaluation of fruit ripeness. In *IEEE Sensors*, pages 1468–1471, New Delhi, India, 2018. IEEE.

[78] Yang, S., Hallett, I., Oh, H. E., Woolf, A. B., and Wong, M. The impact of fruit softening on avocado cell microstructure changes monitored by electrical impedance and conductivity for cold-pressed oil extraction. *Journal of Food Process Engineering*, 42(4):e13068, 2019.

[79] Wang, A.-F., Di, B., Repo, T., Roitto, M., and Zhang, G. Responses of parameters for electrical impedance spectroscopy and pressure–volume curves to drought stress in pinus bungeana seedlings. *Forests*, 11(3):359, 2020.

[80] Jackson, P. J. and Harker, F. R. Apple bruise detection by electrical impedance measurement. *HortScience*, 35(1):104–107, 2000.

[81] Lee, Y., Watanabe, T., Nakaura, Y., Ando, Y., Nagata, M., and Yamamoto, K. Cultivar differences in electrical and mechanical property changes and tolerance in apples due to high hydrostatic pressure treatment. *Postharvest Biology and Technology*, 156:110947, 2019.

[82] Azzarello, E., Mugnai, S., Pandolfi, C., Masi, E., Marone, E., and Mancuso, S. Comparing image (fractal analysis) and electrochemical (impedance spectroscopy and electrolyte leakage) techniques for the assessment of the freezing tolerance in olive. *Trees*, 23(1):159–167, 2009.

[83] Ochandio Fernández, A., Olguín Pinatti, C. A., Masot Peris, R., and Laguarda-Miró, N. Freeze-damage detection in lemons using electrochemical impedance spectroscopy. *Sensors*, 19(18):4051, 2019.

[84] Serrano-Pallicer, E., Muñoz-Albero, M., Pérez-Fuster, C., Masot Peris, R., and Laguarda-Miró, N. Early detection of freeze damage in navelate oranges with electrochemical impedance spectroscopy. *Sensors*, 18(12):4503, 2018.

[85] Romero Fogué, D., Masot Peris, R., Ibáñez Civera, J., Contat Rodrigo, L., and Laguarda-Miro, N. Monitoring freeze-damage in grapefruit by electric bioimpedance spectroscopy and electric equivalent models. *Horticulturae*, 8(3):218, 2022.

[86] Bazihizina, N., Redwan, M., Taiti, C., Giordano, C., Monetti, E., Masi, E., Azzarello, E., and Mancuso, S. Root based responses account for psidium guajava survival at high nickel concentration. *Journal of Plant Physiology*, 174:137–146, 2015.

[87] Muñoz-Huerta, R. F., de J. Ortiz-Melendez, A., Guevara-Gonzalez, R. G., Torres-Pacheco, I., Herrera-Ruiz, G., Contreras-Medina, L. M., Prado-Olivarez, J., and Ocampo-Velazquez, R. V. An analysis of electrical impedance measurements applied for plant N status estimation in lettuce (Lactuca sativa). *Sensors*, 14(7):11492–11503, 2014.

[88] Alejnikov, A., Cheshkova, A., and Mineev, V. Choice of impedance parameter of strawberry tissue for detection of fungal diseases. In *3rd International Conference on Agribusiness, Environmental Engineering and Biotechnologies (AGRITECH)*, volume 548 of *IOP Conference Series: Earth and Environmental Science*, page 032005, Krasnoyarsk, Russia, 2020.

[89] Borges, E., Sequeira, M., Cortez, A., Pereira, H. C., Pereira, T., Almeida, V., Vasconcelos, T., Duarte, I., Nazaré, N., Cardoso, J., et al. Pine decay assessment by means of electrical impedance spectroscopy. In *6th International Joint Conference on Biomedical Engineering Systems*

630 *and Technologies (BIOSTEC)*, Communications in Computer and Information Science, pages 54–73, Barcelona, Spain, 2013. Springer.